AN EXPERIMENTAL AND NUMERICAL INVESTIGATION ON EFFECT OF SHAPES AND ARRANGEMENT OF SOLID BODIES IN WIND LOADING

ZAWAD ABEDIN

DEPARTMENT OF MECHANICAL ENGINEERING

MILITARY INSTITUTE OF SCIENCE AND TECHNOLOGY

MIRPUR CANTONMENT, DHAKA - 1216, BANGLADESH.

October, 2018

AN EXPERIMENTAL AND NUMERICAL INVESTIGATION ON EFFECT OF SHAPES AND ARRANGEMENT OF SOLID BODIES IN WIND LOADING

ZAWAD ABEDIN

(*MSc Engg., MIST*)

A THESIS SUBMITTED

FOR THE DEGREE OF MASTER OF SCIENCE IN

MECHANICAL ENGINEERING

DEPARTMENT OF MECHANICAL ENGINEERING

MILITARY INSTITUTE OF SCIENCE AND TECHNOLOGY

2018

The thesis titled **"An Experimental and Numerical Investigation on Effect of Shapes and Arrangement of Solid Bodies in Wind Loading",** Submitted by **Zawad Abedin**, Roll No: **1016180007**, Session: **April 2016**, has been accepted as satisfactory in partial fulfillment of the requirement for the degree of Master of Science in Mechanical Engineering on 16 October, 2018.

BOARD OF EXAMINERS

…… Professor Dr. Md. Quamrul Islam Department of Mechanical Engineering, MIST Dhaka-1216, Bangladesh	**Chairman** **(Supervisor)**
…… Professor Dr. Mohammad Ali Department of Mechanical Engineering, BUET, Dhaka-1000, Bangladesh	**Member** **(Co-Supervisor)**
…… Col Md. Humayun Kabir Bhuiyan, psc Head, Department of Mechanical Engineering, MIST Dhaka-1216, Bangladesh	**Member** **(Ex-Officio)**
…… Associate Professor Dr. Md. Shahnewaz Bhuiyan Department of Mechanical Engineering, MIST Dhaka-1216, Bangladesh	**Member**
…… Professor Dr. Md. Afsar Ali Department of Mechanical Engineering, BUET Dhaka-1000, Bangladesh	**Member** **(External)**

DECLARATION

I hereby declare that this thesis is my original work and it has been written by me. I have duly acknowledged all the sources of information which have been used in the thesis.

This thesis has also not been submitted for any degree in any university previously.

…….
Zawad Abedin
16 October, 2018

ACKNOWLEDGEMENTS

First of all, my gratitude to Allah for the successful completion of this research work.

I wish to express my sincerest gratitude to Professor Dr. Md. Quamrul Islam, Department of Mechanical Engineering, MIST for his guidance and supervision. His encouragement and invaluable suggestions are gratefully acknowledged.

I also want to express my deepest gratitude to Professor Dr. Mohammad Ali, Department of Mechanical Engineering, BUET for his constructive suggestion and advice during several phases of this problem.

Special thanks to Md. Ali Noor, Senior Technical Officer of Fluid Mechanics Laboratory of Mechanical Engineering Department of BUET, Dhaka for his kind cooperation in constructing, fabricating and assembling different parts and components of the experimental set-up. Also I acknowledge the cooperation and invaluable assistance in different aspects of the entire work offered by Wing Commander Dr. Vikram Deshpande, Indian Air Force, Department of Aeronautical Engineering, Sqn Ldr Mst Mousumi Rizia (Retd), Md. Tanvir Ehsan and Lecturer Atif Yasir of Department of Mechanical Engineering, MIST.

Finally, I would like to express my sincere thanks to all members of the Department of Mechanical Engineering of MIST for their cooperation and help in the successful completion of the work.

LIST OF CONTENTS

ABSTRACT

In this research, an experimental and numerical investigation regarding effect of shapes and arrangement of solid bodies in wind loading is carried out. The study was performed on the group consisting of three cylinders, arranged in staggered form, one square cylinder in the downstream and another two hexagonal and pentagonal cylinder in the upstream side. Also simulation was done using simulation software package keeping the arrangement and geometry same. The test was conducted in an open circuit wind tunnel at a Reynolds number of 4.89 x 10^4 based on the face width of the cylinder across the flow direction in a uniform flow velocity of 14.3 m/s. The experimental work was carried out on a staggered form at various angles of attack which are 0°, 30°, 45°, 60° respectively. The surface static pressures at the different locations of the cylinder were measured with the help of inclined multi-manometers. The pressure coefficients were calculated from the measured values of the surface static pressure distribution on the cylinder. Later the drag and lift coefficients were obtained from the pressure coefficients by the numerical integration method. The wind flow effect on the cylinders in staggered form was simulated using Fluent as solver. The results specially the simulation technique will enable the engineers and architects to design buildings more efficiently. Since the results are expressed in the non-dimensional form, they might be applied for the prototype buildings as well.

LIST OF TABLES

LIST OF FIGURES

NOMENCLATURE

h_a	Air head
P_o	Ambient pressure
α	Angle of attack
$\acute{\omega}$	Angular velocity of the earth
C_D	Coefficient of drag
C_L	Coefficient of lift
C_p	Coefficient of pressure
P	Density of air
F_D	Drag force
U_∞	Free stream velocity
A	Frontal area of the Cylinder
Z	Height
X	Latitude velocity of the earth
F_L	Lift force
L_1	Longitudinal distance between two cylinders
Δh_w	Manometer reading
ΔP	Pressure difference
dp/dn	Pressure gradient
γ_a	Specific weight of air
γ_w	Specific weight of manometer liquid (water)
P	Static pressure on the surface of the cylinder
L_2	Transverse distance between two cylinder
V	Wind speed

CHAPTER-1

INTRODUCTION

1.1 General

Wind is caused by air flowing from high pressure to low pressure region. Since the Earth is rotating, air is deflected to the right (in the Northern Hemisphere; to the left in the Southern Hemisphere), so that the wind flows mostly around the high and low-pressure areas.

Wind is one way that the atmosphere dissipates excess heat around. Wind forms for the primary purpose of helping to transport excess heat in one of two ways: away from the surface of the Earth or from warm regions (tropics) to cooler regions. Friction from the ground slows the wind down. During the day convective mixing minimizes this effect, but at night (when convective mixing has stopped) the surface wind can slow considerably down, or even stop altogether.

The subjects of wind load on buildings and structures are very old. In the 17thcentury, Galileo and Newton have considered the effect of wind loading on buildings, but during that period it did not gain popularity. The effect of wind loading on buildings and structures has been considered for design purposes since late in the 19th century; but starting from that time up to about 1950, the studies in this field have not been considered seriously. Calculation of wind loads is important in the design of wind force resisting system, including structural members, components, and cladding against shear, sliding, overturning, and uplift actions.

In recent years, much emphasis has been given on the study of wind effect on buildings and structures in the different corners of the world. Even researchers in Bangladesh have taken much interest in this field. Till now, little attention has been paid to the flow over the bluff bodies like square cylinders, rectangular cylinders, hexagonal cylinders, octagonal cylinders etc. and some information is available concerning the flow over them in staggered condition, although this is a problem of considerable practical significance. With the progressing world, engineering problems regarding wind loads around a group of skyscrapers, chimneys, towers and the flow induced vibration of tubes in heat exchangers, bridges, oil rigs or marine structures need detailed investigation of flow patterns and aerodynamic characteristics.

Arising from the increasing practical importance of bluff body aerodynamics, over the past few decades' sufficient effort has been given in research works concerning laboratory simulations, full-scale measurements and more recently numerical calculations and theoretical predictions for flows over bodies of wide variety of shapes. A number of failures of bridges, transmission towers, buildings and housings over the last one hundred years prompted researchers to do research work in this field. Some of the pioneer researchers in the field are Smeaton (1759), Vogt (1880), Irminger (1891), Eiffel (1900) and Stanton (1907).

Irminger in 1891 published results of measurements on models, which was probably the first-ever wind tunnel test and Eiffel in the period up to 1900. This was followed by the completion of the famous tower, conducting pioneer studies on the flow velocities and tower movements from a laboratory at the top of the tower.

The study of wind effect was first limited to loading on buildings and structures only, possibly because of its most dramatic effects are seen in their collapses. In mid-sixties, researchers started the study of less dramatic, but equally important environmental aspects of flow of wind around buildings. These include the effects on pedestrians, weathering, rain penetration, ventilation, heat loss, wind noise and air pollution etc. The pioneer researcher in this field is Lawson, T. V. of the University of Bristol. A number of works of the environmental aspects of wind was being studied at the Building Research Establishment at Garson and the University of Bristol, U. K.

It is true that researchers from all over the world have contributed greatly to the knowledge of flow over bluff bodies. but the major part of the reported works is of fundamental nature involving the flow over single body of different profiles. Most of the researchers have conducted works either on single cylinder with circular, square, octagonal, hexagonal or rectangular sections etc. or in a group with them for various flow parameters. However, the flow over a combination of square, pentagonal and hexagonal cylinders has not been studied extensively especially in-groups till date, although this is a problem of practical significance. It is believed that the study on the cylinder with square, pentagonal and hexagonal section will contribute to find the wind load on the single and group of square, pentagonal and hexagonal buildings and the results will be useful to the relevant engineers and architects.

1.2 Nature of the Wind

Very strong winds are generally associated with cyclonic storms, thunderstorms, dust storms or vigorous monsoons. A feature of the cyclonic storms over the Bangladesh region is that they rapidly weaken after crossing the coasts and move as depressions. The influence of a severe storm after striking the coast does not in general exceed about 60 kilometers, though sometimes, it may extend even up to 120 kilometers. The wind behavior is discussed in this section in brief. The characteristics of the wind, which are more or less related to the present study, have been taken into consideration for discussion.

1.2.1 Wind Velocity

High wind velocity is responsible for the failure of building and structures and it can cause unpleasant side effects. Strong winds often have special names, including gales, hurricanes and typhoons. The wind speeds recorded at any locality are extremely variable and in addition to steady wind at any time, there are effects of gusts, which may last for a few seconds. Because of the inertia of the building, short period gusts may not cause any appreciable increase in stress in main components of the building and structure. The response of a building to high wind pressures depends not only upon the geographical location and proximity of other obstructions to airflow but also upon the characteristics of the structure itself.

Winds are named by the direction they come from. Thus, a wind from south, blowing toward the north is called a south wind. Windward refers to the direction a wind comes from, leeward to the direction it blows toward. When a wind blows more frequently from one direction than from any other it is called a prevailing wind. Wind speed increases rapidly with height above the ground level, as frictional drag declines. Wind is commonly not a steady current but is made up of a succession of gusts, slightly variable in direction, separated by pauses. Close to the earth the gustiness is developed due to irregularities in the wind are caused by the conventional currents. All forms of turbulence play a part in the process of transporting heat, moisture and dust into the air aloft.

There are various parameters, which control the flow behavior such as (i) vortices in front of the building, (ii) opening through buildings, (iii) spacing of rows, (iv) wakes of buildings, (v) long straight streets, (vi) narrowing streets, (vii) corners and (viii) courtyards. The mean wind speed varies with height. The variation of wind speed is expressed as

$$V = V_c(Z/Z_c)^a \tag{1.1}$$

where, V is the mean wind speed at a height Z, V_c is the mean wind speed at the gradient height Z_c. The value of V_c depends upon the geographical locality, but Z_c is a function of terrain. Values of Z_c and the exponent 'a' suggested by Davenport, A. G. [14] are as follows:

For open terrain with very few obstacles: $a = 0.16$, $Z_c = 300$m

For terrain uniformly covered with obstacles 10-15 in height: $a = 0.28$, $Z_c = 430$m

For terrain with large and irregular objects: $a = 0.40$, $Z_c = 560$m

1.2.2 Generation of Wind

The source of wind energy is the sun that emits solar radiation, which causes differential heating of the earth surface and the atmosphere. In the atmosphere there is a general convective transport of heat from lower to higher latitudes in order to make the earth's radiation imbalance. It is for this reason that the atmosphere is a restless medium in which circulation of all sizes is normal. Wind is simply air moving in a direction that is essentially parallel with the earth's surface. The atmosphere is fixed to the solid-liquid earth (land and water portion) in gravitational equilibrium and so moves with the earth in its west to east rotational movement. Wind, therefore is air movement in addition to that associated with rotation. In large-scale circulation covering several thousand miles, horizontal motion greatly exceeds vertical motion. Thus, a wind that takes several days to cross an ocean may move up or down only a few miles. The vertical component of movement is much greater in small-scale circulation such as thunderstorms and tornadoes. In a thunderstorm, air may ascend to the top of the atmosphere in about an hour.

Wind is complex in origin. Usually, its direct cause lies in differences between atmospheric densities resulting in horizontal differences in air pressure. That is, it represents nature attempt to rectify pressure inequalities. When these horizontal pressure differences develop, a gradient of pressures exists. But in spite of the direct part played by pressure differences, the ultimate source of average for generating and maintaining winds against the drag is mainly from the differences in heating and cooling between high and low latitudes.

1.2.3 Forces Governing Winds

Four forces operate to determine the speed and direction of winds: (i) Pressure gradients force, (ii) Coriolis force, (iii) Frictional force and (iv) Centrifugal force.

i) Pressure Gradient Force

This sets the air in motion and causes it to move with increasing speed along the gradient. The magnitude of the force is inversely proportional to the isobar spacing. Since the gradient slopes downward from high to low pressure, direction of airflow is from high to low pressure along the pressure gradient. But due to the rotation of the earth, the trajectory of an air particle moving from high to low pressure is very indirect, except close to the equator.

ii) Coriolis Force

This is the deflecting force of the earth's rotation that affects only the direction of wind. Except at the equator, winds and all other moving objects, no matter what their direction, are deflected to the right of the gradient in the northern hemisphere and to the left in the southern hemisphere. The force acts at right angles to the direction of motion. Coriolis force is stronger in higher latitudes. When pressure gradient is balanced by the Coriolis force, wind blows parallel with the isobars and it is called geotropic wind. The geotropic wind V_c can be estimated from the expression:

$$V_c = (dp/dn)\,(2\rho\omega\, sin\, x) \qquad (1.2)$$

where (dp/dn) is the pressure gradient, ω is the angular velocity of the earth, x is the latitude and ρ is the air density. Outside the atmosphere friction layer may be extended up to 1000m above the earth's surface. Wind actually does blow in a direction almost parallel with the isobars with low pressure on the left and high pressure on the right in the northern hemisphere.

iii) Frictional Force

This affects both wind speed and direction. Friction between the moving air and the earth's land-sea surface tends to slow the movement of air. Because of the frictional effects of the land-sea surface upon air flowing over it, surface air does not flow essentially parallel with the isobars as it does aloft, but instead crosses them at an oblique angle. The greater the friction, the wider is the angle the wind direction makes with the isobars. Winds over irregular land surfaces usually form angles varying from 20^0 to 45^0 with the isobars. But over oceans, the angle may be as little as 10^0.

iv) Centrifugal Force

This force comes into picture only when air moves in a curved path. Centrifugal force is a major factor only when the wind is strong and the radius of curvature small as they are in tropical hurricanes, tornadoes and the centers of a few usually well-developed cyclonic storms. The flow of air which is necessary to balance pressure force, Coriolis force and centrifugal force in absence of frictional force is called gradient wind. This happens at heights greater than 500 m or so.

1.3 Wind Loading on Structures

The effect of wind on the structure as a whole is determined by the combined action of external and internal pressures acting upon it. In all cases, the calculated wind loads act normal to the surface to which they apply. The pressures created inside a building due to access of wind through openings could be suction (negative) or pressure (positive) of the same order of intensity while those outsides may also vary in magnitude with possible reversals. Thus, the design value shall be taken as the algebraic sum of the two in appropriate/concerned direction. Furthermore, the external pressures (or forces) acting on different parts of a framework do not correlate fully. Hence, there is a reduction in the overall effect.

The development of modern materials and construction techniques has resulted in the emergence of a new generation of structures. Such structures exhibit an increased susceptibility to the action of wind. Accordingly, it has become necessary to develop tools enabling the designer to estimate wind effects with a higher degree of refinement than has been previously required. It is the task of the engineer to ensure that the performance of structures subjected to the action of wind will be adequate during their anticipated life from the standpoint of both structural safety and serviceability. To achieve this end, the designer needs information regarding (i) the wind environment, (ii) the relation between that environment and the forces it induces on the structures and (iii) the behavior of the structure under the action of forces.

The action of wind on building considering the load effect may be classified into two major groups; the static effect and the dynamic effect. There are many other effects like generation of noise the risk of the hazard, the penetration of rain and uncomfortable wind for the pedestrians etc. but they are not usually considered for structural design. Since all wind

loadings are time-dependent because of varying speeds and direction of winds, wind loading is never steady. For this reason, static load is referred to the steady (time-variant) forces and pressures tending to give the structure a steady displacement. On the other hand, dynamic effect has the tendency to set the structure oscillating. A steady wind load on a building is very difficult to achieve. In fact, always wind loads are of a fluctuating nature because of varying speeds and directions of winds. The type of wind and the stiffness and roughness of the structure determine the nature of loading on a building. When a building is very stiff the dynamic response of the structure may be neglected and only the static leads may be considered. This is because the natural frequency of an extremely stiff building is too high to be excited by wind. In the present study, the effect of static loading is taken into account due to the steady wind. Since natural winds are continually fluctuating, it is generally assumed that these fluctuations are so irregular and random that the response of a structure will not differ from that due to a steady wind of the same average speed. Very recently the dynamic response of building has been considered for study because of the modern tendency to build slenderer and lighter structures.

1.4 Necessity of the Study

In Bangladesh, strong wind is an annual natural hazard due to its geographical location. On the other hand, most of the existing houses and those which are going to be built in the next few decades are likely to be non-engineered, mostly with thatched roofs and are vulnerable to wind. Strong wind is causing immense losses of rural dwellers by making their houses collapse fully or partially by lifting of roof etc. Almost 70% of the population in the rural sector and 50% of the population in the urban sector are living below the poverty level with earnings too little to pay for all needs. It is this group of people most impoverished that is to be provided with good housing. About 75% of the dwelling in rural areas is of kutcha construction (Mud, Bamboo, Woven Bamboo etc.) and that 23% of urban and more than 40% of rural dwellings are of a temporary nature. They can rarely survive against even a moderate intensity storm. Evidence from the field in strong wind-prone areas indicates that there is a socially perceived need of more engineering knowledge and improved construction of domestic dwelling.

Bangladesh is a country having scarcity of land. The urban population of this country is increasing at a very fast rate making the housing problem worse every day. One possible solution of the housing problem is to construct multistoried buildings. The knowledge of wind

loading on a single tall building or on a group of tall buildings is essential for their economic design. The flow around a combination of square, pentagonal and hexagonal model cylinder can be ideally considered analogous to that of the flow around a combination of tall square, pentagonal and hexagonal shaped building. Therefore, a study of wind flow around groups of square, pentagonal and hexagonal cylinders would be helpful in this respect. For designing groups of tall buildings, knowledge of the effect of wind loading on a single tall building is not sufficient because the effects of nearby buildings on the loads imposed on a structure would be quite different. In the areas with high rise buildings, other problems like unpleasant wind conditions may be developed near ground level in passages between and through buildings and many instances of such conditions, causing discomfort for the pedestrians and damage to doors and windows in and near the passage have been reported. In order to eliminate these nuisances, architects and town planners of Bangladesh should have a better knowledge of the wind flow around the buildings, which can save the nation from making both loss of lives and properties. In the present study, it has been tried to give an understanding about the variation of wind load pattern imposed on building due to the influence of the nearby buildings. To find the complete solutions of the above-mentioned problems a more detailed study in this regard is needed.

There are many examples of failures of buildings and structures in different parts of the world, which has made the enthusiastic investigators puzzled to find the exact causes, and research works are being carried out to find the proper remedial measures for eliminating these failures. The investigators of this country may contribute a lot to the nation by conducting appropriate research work in this field.

Though the problem regarding the wind loadings on buildings and structures is common to all parts of the world and it is expected that the solution will not be significantly different from country to country, yet research work should be carried out in this field considering the climatic conditions and problem of this country so that a clear picture about the nature of wind loading can be obtained. The data from these research works should enable to the architects, engineers and town planners of Bangladesh to design buildings and structures more efficiently.

1.5 Importance of Model Study

Differences between wind tunnel and full-scale result can occur due to Reynolds number inequality, incorrect simulation of the atmospheric boundary layer and small-scale difference

between wind tunnel and prototype model. In most wind tunnels tests the full-scale Reynolds number is rarely achieved. Boundary layer separation depends on Reynolds number. For sharp edged structures, separation point does not depend on Reynolds number. On the other hand, the flow field around curved surfaces are very much Reynolds number dependent, so tests on these configurations must be treated with care the crosswind scales in wind tunnels are often less than reality. This can cause underestimation of cross wind effects. The scale difference between wind tunnel model and prototype is found in the high frequency fluctuation. High peaks found on the cladding in full-scale are not found in the wind tunnel. Those effects may be caused by structural details that are not simulated in the wind tunnel model.

Now-a-days, both the studies with models and full-scale buildings are being performed to compare the result for varying the validity of the former. But full-scale experiments are both costly and difficult to perform. For the present study with staggered buildings full-scale experiments will not only be complex and costly but also it would be difficult to record reliable pressure distribution simultaneously on the group of buildings as there will be variation of speeds and direction of wind with time. The flow around buildings in actual environment is very complex and formulation of a mathematical model to predict the flow is almost impossible. Thus, model study is a must and the results obtained under simulated condition in the laboratory are found to be quite satisfactory for practical purposes.

1.6 Objective of this research

In the present experimental and numerical investigation, square, pentagonal and hexagonal cylinders with a combination will be taken into consideration. The objectives of the study are as follows:

a) To measure the pressure distribution around square, pentagonal and hexagonal cylinders at different angle of attack
b) To determine the following parameters from static pressure distributions i.e. the wind loading of the cylinders- Coefficient of Pressure (C_P), Coefficient of Drag (C_D) and Coefficient of Lift (C_L).
c) To compare the experimental results with the 2-D simulation outcome using Ansys 16.

It is expected that the wind load on the square, pentagonal and hexagonal combination will be comparable to that with the same type of cylinders. The result will enable the engineers and architects to design buildings more efficiently. Since the results will be expressed in the non-dimensional form, they may be applied for the prototype buildings.

CHAPTER-2

REVIEW OF LITERATURE

2.1 General

In the past, there were some occurrences of disastrous collapse of suspension bridges and damages to buildings and structures, which made the relevant researchers to pay attention for performing researches in the field of wind loading on structures and buildings. Many researchers carried out work mainly on isolated bluff bodies primarily. Later, they started conducting work on group of buildings and structures. They also carried out the research work about the effect of environment on the buildings in parallel. Information concerning the flow over staggered square, pentagonal and hexagonal cylinders is not probably available in detail, although this is a problem of practical significance. In this chapter, a brief description of some of the works related to the problem will be mentioned.

2.2 Existing Work on Wind Loading:

Baines [1] presented in his paper the effects of velocity distribution on wind loads and flow patterns around buildings. He measured pressure distributions on models of walls and rectangular block structures in a wind tunnel. Tall buildings with square sections have also been included in his study. The tests were conducted both in an artificially produced velocity gradient used to simulate natural conditions and in a constant velocity field for comparison with standard procedures.

Barriga et al. [2] studied the effects of angle of attack, turbulence intensity and scale on the pressure distribution of a single square cylinder placed in a turbulent cross flow. They found that when the square cylinder was positioned in a cross flow with one face normal to the flow direction, only drag force was produced, but in the same flow a negative lift force was developed at small positive angle of attack, the magnitude of which was depended on the turbulence characteristics of the cross flow. It was suggested that the negative lateral forces on the square cylinder oriented at a small positive angle of attack was due to the relatively large negative pressure co-efficient in the separated zone on the windward side wall. It was also concluded that the effect of turbulence intensity was to decrease the pressure near the

front corner of the windward side wall and promote flow reattachment near the rear, giving rise to a very significant increase in aerodynamic moment.

Bearman et al. [3] presented in their paper how the flow around two circular cylinders, displaced in a plane normal to the free stream, interacts as the two bodies are brought close together. Surface pressure measurements at a Reynolds number of 25000 based on the diameter of a single cylinder (d), showed the presence of a mean repulsive force between the cylinders. At gaps between 0.1d and 1d a marked asymmetry in the flow was observed with the two cylinders experiencing different drags and base pressures. The base pressure was found to change from one steady value to another or simply fluctuated between the two extremes. It was also showed how mutual interference influenced the formation of vortex streets from the two cylinders.

Biswas [4] performed an experimental investigation of wind load on tall buildings with square cross section having rounded facet in a uniform flow. Five different facet dimensions were considered in the study. The study included both the single cylinder and the group consisting of two cylinders. The inter spacing between the cylinders in the group were also varied. The test was conducted in an open circuit wind tunnel at a Reynolds number of 54000 based on the face width length across the flow. It was found that there is remarkable effect of rounded facet on the drag coefficient.

Bostock et al. [5] studied the pressure distributions and forces on rectangular and D-shaped cylinders placed in two-dimensional flow with a Reynolds number of 190000. It was found that for rectangular cylinders a maximum drag coefficient was obtained when the height (normal to the stream) of the section was about 1.5 times the width. Reattachments on the sides of the cylinders occurred only for height diameter ratio less than 0.35.

Castro et al. [6] described in their paper the flow around surface mounted cubes in uniform, irrigation and sheared turbulent flows. The shear flow was simulated atmospheric boundary layer with a height ten times of the body dimensions. They presented measurements of body surface pressure and mean and fluctuating velocities within the wake region. These measurements reflected the effects of upstream turbulence and shear on the wake flow. It was found that in the reversed flow region directly behind the body the addition of upstream turbulence and shear considerably reduced the size of cavity zone. Unlike the case of uniform flow the separating shear layers reattached to the body surface. Measurements for a variety

of cube size boundary layer height ratio further revealed that reattachments occurred even for cube heights larger than the boundary layer height. They found that in the case of uniform flow approaching the cube at 45 degrees, the near wake and pressure fields were dominated by strong vortex shed from the top edge of the body.

Islam et al. [7] conducted an experimental investigation of static pressure distributions on a group of rectangular cylinders in a uniform cross flow. They determined the effects of longitudinal spacing and side dimension of the rectangular cylinders. Finally, the lift and drag coefficients were calculated from the measured data of surface static pressure.

Farok [8] carried out an experimental investigation of wind effect on rectangular cylinders with rounded corners. Both the single cylinder and group of cylinders were considered in that study. It was observed that with the rounded corners the drag on the cylinders reduces remarkably in comparison to that on the sharp-edged cylinders. The effect of inter-spacing is also considered in their study.

Hua [9] conducted the measurements of fluctuating lift and the oscillating amplitudes on a square cylinder in a wind tunnel test.

Davis et al. [10] carried out a numerical study of vortex, shedding from rectangular cylinders. They attempted to present numerical solutions for two-dimensional time dependent flow about rectangles in infinite domains and investigated the initiations and subsequent development of the vortex shedding phenomena for Reynolds number varying from 100 to 2800. It is found that the properties of these vortices were strongly dependent on the Reynolds number. Lift, drag and Strouhal number were also found to be influenced by Reynolds number.

Lee [11] conducted the study of the effect of turbulence on the surface pressure field of a square prism and measurements of the mean and fluctuating pressures on a square cylinder placed in a two-dimensional uniform and turbulent flow. It was observed that the addition of turbulence to the flow raised the base pressure and reduced the drag of the cylinder. It was suggested that this phenomenon was attributable to the manner in which the increased turbulence intensity thickened the shear layers, which caused them to be deflected by the downstream corners of the body and resulted in the downstream movement of the vortex formation region. The strength of the vortex shedding was shown to be reduced as the intensity of the incident turbulence was increased. Measurements of drag at various angles of

attack (0° to 45°) showed that with increase in turbulence level the minimum drag occurred at smaller values of angle of attack.

Mandal et al. [12] presented a paper on static pressure distributions on the cylinder with either square or rectangular cross-section having rounded corners. The experiment was performed for different corner radii and side dimensions of the cylinders at zero angle of attack. The wind load decreased appreciably for the cylinder with rounded corner compared to that with sharp corner. The experimental results reveal that the corner radius of the cylinder has significant effect while the side dimension has small effect on the drag coefficient.

Hussain et al. [13] measured coefficient of pressure and coefficient of lift on circular, parabolic and elliptic shell roof in a uniform velocity. The investigation was performed in a small wind tunnel. As the experiment was carried out in a uniform velocity, the estimated results would be higher than that in reality.

Hossain et al. [14] made an experimental investigation of wind effect on staggered cylinders of square and rectangular sections with variable longitudinal spacing. In the paper it was found that there is significant effect of inter-spacing on the wind load of cylinders.

Islam et al. [15] performed an experimental investigation of surface static pressure distributions on rectangular cylinders for a uniform cross-flow. The surface static pressure distribution was measured and the drag and lift coefficients were obtained. For all side ratios of the rectangular cylinders it was observed that the minimum drag occurred within 8^0 and 12^0 angle of attack.

Islam et al. [16] presented a paper on surface static pressure distributions on a group of rectangular cylinders for a uniform cross flow considering the effect of side ratios and longitudinal spacing on pressure distribution. The drag and lift coefficients were obtained from the measured surface pressure distribution. It is observed that with the increase of the side ratio the drag coefficients increased in general.

Koeing et al. [17] described in the paper an experimental investigation of the shielding effects of various disks placed co-axially upstream of an axisymmetric flat faced cylinder. For certain combinations of the diameter and gap ratios they observed a considerable decrease in the drag of such a system. By flow visualization technique they showed that for such optimum

shielding the upstream surface, which separated from the disk reattached smoothly onto the front edge on the downstream cylinder.

Leutheusser [18] made wind tunnel tests on scale models of typical building configurations. The experiment was conducted on four models each with different height and cross-section. The static wind loading was found on each of the buildings in free standing condition and as a member of a group of buildings. It was concluded that the wind loading of a building was less severe when is formed a part of a group than when it was free standing.

Mandal et al. [19] measured the static pressure distributions on a group of cylinders with either square or rectangular cross-section having rounded corners. The experiment was performed for a group consisting of two cylinders one behind the other along the flow direction with different side dimensions at zero angle of attack for various inter-spacing between the cylinders. It is observed from the experimental results that there is appreciable effect of the side dimension and interspacing on the drag coefficient of the cylinders. The results are applicable to a group consisting of two tall buildings one behind the other along the wind velocity direction and each building of either square or rectangular cross-section having rounded corners.

Mandal et al. [20] made a study of wind effects on a group of square cylinders with variable longitudinal spacing. The test was conducted in an open circuit wind tunnel at a Reynolds number of 27800 based on the side dimension of the square model. The maximum blockage area was 6.96 percent. Three cylinders were arranged in the staggered form (one in upstream and two in downstream side) varying the longitudinal and transverse spacing and measurements of pressure coefficients were taken for the upstream and downstream cylinders. Experiments were also carried out for drag coefficients, lift coefficients, total force coefficients and moment coefficients. After all, it was concluded from the results that wind loading on a building is generally less severe when the building forms part of a group than when it is free-standing.

Mandal et al. [21] performed an experimental investigation of wind effect on staggered square cylinders with variable transverse and longitudinal spacing. They measured the surface static pressure distributions of each of the cylinders and then they calculated the drag and total force coefficients from the static pressure. It was observed that the net wind load on the individual

cylinder of the group decreased in general; however, there appeared high local pressure coefficient in some cases.

Matsumoto [22] made an investigation on the aerodynamic forces acting on an oscillating square prism in a steady flow both experimentally and theoretically. First, a few experiments were performed to examine the aerodynamic forces in the direction of the wind stream and in a plane normal to it, acting on an oscillating square prism. Karman's theory about a thin plate was extended to the case of a square prism and the aerodynamic forces in a plane of the direction of the wind stream were obtained. Good correlation was found between the theoretical and experimental results.

Nakamura et al. [23] made experimental investigation on the vortex excitation of rectangular cylinders with the long side normal to the flow in a mode of lateral translation using free and oscillation methods.

Nakamura et al. [24] studied the effects of turbulences on the mean flow past square rods. Measurements were made on square rods with different lengths with their square face normal to the flow to investigate the effects of turbulence intensity and scale on the mean flow characteristics. The turbulence intensity varied from 3.5% to 13% and the length to size ratio of the rods ranged from 0.1 to 2.0. It was found out that there were two main effects of turbulence on the mean flow past a three-dimensional sharp edged bluff body. Small-scale turbulence increased the growth rate of the shear layer, while the large-scale turbulence enhanced the roll up of the shear layer. For a square plate, both small and large-scale turbulence reduced the size of the base cavity. As the length of the square rod was increased beyond the critical (0.6 times the heights), the shear-layer-edge direct interaction controlled the near wake eventually leading to flow reattachment. The effect of small scale turbulence was to promote the shear layer direct interaction.

Nakamura et al. [25] attempted to study vortex shedding from square prisms placed to smooth and turbulent approaching flows. A flow visualization was made and the velocity and pressure for the flow past prism of variable length with square section was measured. It was found that square prisms shed vortices in one of the two-fixed wake planes, which were parallel with the plate sides. The plane of shedding was switched irregularly from one to the other.

Roberson [26] carried out experiments on circular cylinders, spool shaped bodies, cup-shaped bodies, square rods and rectangular rods to observe the effect of turbulence on the drag of

these bodies. For square rods with their axes parallel to the flow direction it was found the C_d decreased approximately 25% when the turbulence intensity increased from 1% to 10%. Two rectangular rods used; one had a square cross-section and the other had a length (in the free stream direction) to breadth ratio of two. The drag was measured with the axes of the rectangular rods oriented normal to the free stream direction. It was noted that on the sides of the square rod the pressure change with a change in turbulent intensity was about the same as for the face; while for the rectangular rod, the change in pressure on the sides was large, and it was small on the rear face. The conclusion was that the bodies, which have shapes such that reattachment of the flow is not a factor, experience an increase in C_d with the increased turbulence intensity. On the other hand, bodies for which reattachment or near reattachment of flow occur with increased turbulence may experience either a decrease or increase in C_d with increased turbulence intensity depending upon the shape of the body.

Roberson [27] measured pressure distribution on rectangular rods placed in a cross flow with the rods oriented at small angle of attack with respect to the direction. The Reynolds number based on the minimum dimension of the rod was 40000 and the turbulence intensity of the cross flow ranged between 1% and 10%. The conclusion was that the free stream turbulence had a significant effect on the pressure distribution about bodies of rectangular cross-section. With small angle of attack these bodies had a significantly lower pressure on their windward side wall than did the same bodies with zero angle of attack. To study the pressure distributions on bodies that more nearly represents building configurations, tests were made on bodies of square cross-section placed on the floor of the wind tunnel. It was found that decreasing relative height of the body had an attenuating effect on the negative pressure on the windward side wall and it also increased the critical angle of attack.

Sakamoto et al. [28] collected experimental data on the vortex shedding frequency behind a vertical rectangular prism and a vertical circular cylinder attached to a plane wall and immersed in a turbulent boundary layer. They tried to investigate the effects of the aspect ratio (height/width) of these bodies and the boundary layer characteristics on the vortex shedding frequency. Measurements revealed that two types of vortex were formed behind the body, depending on the aspect ratio; they were the arch-type vortex and the Karman-type vortex. The arch-type vortex appeared at an aspect ratio less than 2.0 and 2.5 for rectangular and circular cylinders respectively. The Karman type vortex appeared for the aspect ratio

greater than the above values. The whole experiment was conducted at a turbulence level of 0.2% and free stream velocity of 20 m/s. The aspect ratio was varied from 0.5 to 0.8.

Vickery [29] presented in his paper the results of the measurements of fluctuating lift and drag on a long square cylinder. He attempted to establish a correlation of lift along the cylinder and the distribution of fluctuating pressure on the cross-section. The magnitude of the fluctuating lift was found to be considerably greater than that for a circular cross-section and the span wise correlation much stronger. It was also reported that the presence of large-scale turbulence in the stream had a remarkable influence on both the steady and the fluctuating forces. At small angle of attack (less than 10°) turbulence caused a reduction in base suction and a decrease in fluctuating lift of about 50%.

Besides these, many authors have performed study on flow patterns, wind loads and their effects on buildings and structures, which have been mentioned in the references.

Besides the above research works, many other works have also been done by many researchers in the different places, but very few have taken the combination of square, pentagonal and hexagonal cylinders together for study. Especially the square, pentagonal and hexagonal cylinders in staggered condition have not been included for finding the wind load. Thus, this study would definitely add to the new idea in regard to the wind loading for tall buildings.

CHAPTER-3

EXPERIMENTAL SET-UP

3.1 General

The experimental investigation to find wind load on the square, pentagonal and hexagonal cylinders in staggered form was conducted at the exit end of a subsonic open circuit wind tunnel. The test was done on a group consisting of one square cylinder in the downstream side and a pentagonal and hexagonal cylinders in the upstream side in a uniform cross flow. The surface static pressures at the different locations of the cylinder were measured with the help of an inclined multi-manometer. In this chapter a brief description regarding the construction of the cylinders, the wind tunnel, the testing procedure etc. has been provided systematically.

3.2 Wind Tunnel

The test was done in an open circuit subsonic wind tunnel as shown in Figure 3.1. It was the low speed wind tunnel having the maximum wind velocity of 14.3 m/s in the test section. The tunnel consists of various components such as, fan, valve, silencer, honey comb etc. It is 5.93-meter-long with a test section of 460-mm x 460 mm cross-section. In order to make the flow uniform a honeycomb is fixed near the end of the wind tunnel. There is a converging bell mouth shaped entry. To generate the wind velocity, two axial flow fans are used.

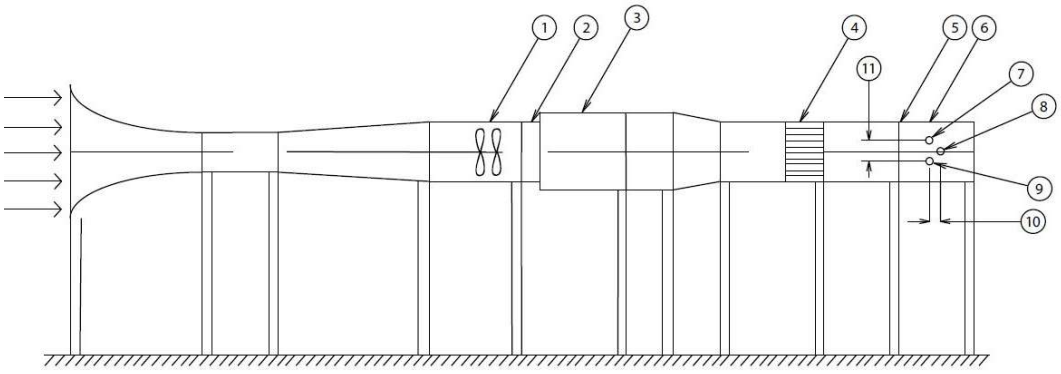

1. Fan section
2. Valve section
3. Silencer
4. Exit end
5. Test section
6. Honey comb
7. Pentagonal cylinder
8. Square cylinder
9. Hexagonal cylinder
10. Longitudinal spacing, L_1
11. Transverse spacing, L_2

Figure 3. 1: Schematic diagram of wind tunnel [12]

Each of the fans is connected with the motor of 2.25 kilowatt and 2900 rpm. There is a butterfly valve to control the wind speed. There is a silencer just after the butterfly valve as shown in the figure.

The central longitudinal axis of the wind tunnel is maintained at a constant height of 990 mm from the floor. The axis of the model coincides with that of the wind tunnel. The converging mouth entry is incorporated in the wind tunnel for smooth entry of air into the tunnel and to maintain uniform flow into the duct free from outside disturbances. The induced flow through the wind tunnel is produced by two-stage rotating axial flow fan of capacity 18.16 m^3/s at the head of 152.4 mm of water and 1475 rpm.

A butterfly valve, actuated by a screw thread mechanism, is placed behind the fan and used to control the flow. A silencer is fitted at the end of the flow controlling section in order to reduce the noise of the system. This section is incorporated with a honeycomb. The diverging and converging section of the wind tunnel is 1550 mm long and made of 16 SWG black sheets. The angle of divergence and convergence is 7°, which has been done with a view to minimizing expansion and contraction loss and reducing the possibility of flow separation.

In each case of the tests, wind velocity is measured directly with the help of a digital anemometer. The flow velocity in the test section 14.3 m/s approximately. The measured velocity distribution was almost uniform across the tunnel test section in the upstream side of the test models. The pattern of the flow velocity is shown in Figure 3.2 in the non-dimensional form.

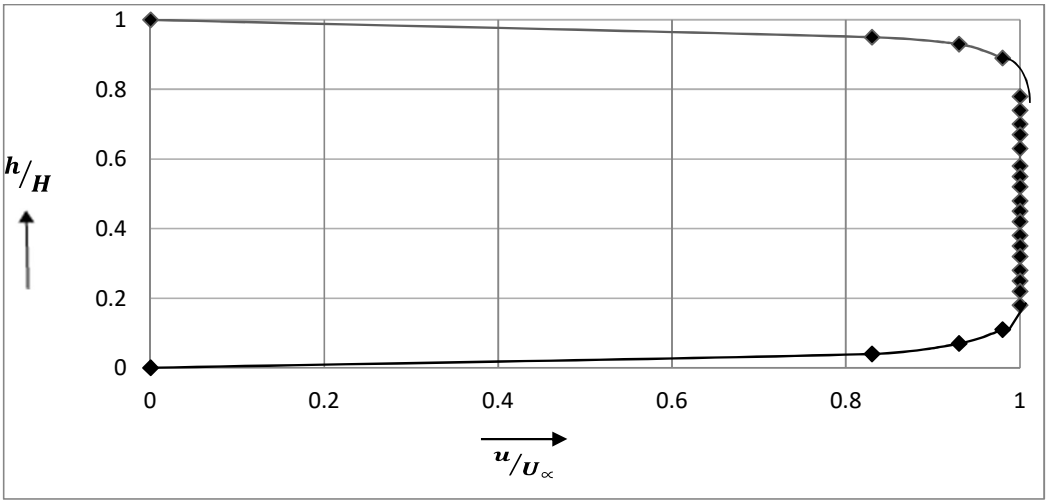

Figure 3. 2: Velocity distribution at upstream side of model

3.3 Test Section

In reality the test was done at the exit end of the wind tunnel in the open air as shown in Figure 3.1. In order to fix the cylinder a steel frame was fabricated, the top floor of which was at the same level of the wind tunnel at the exit end. Two side walls were attached to the steel frame at the two sides by the help of nut and bolt. The distance between the extended side walls was equal to the distance of the side walls of the wind tunnel exit end. This distance of between the side walls was 460 mm. The length of the test section was 400 mm. There was no cover plate at the top and bottom of the extended test section.

The cylinders were fixed with the extended sidewalls. The sidewalls were made of plywood. In one side, the model cylinder was fastened with the side wall using nut and bolt. The bolt was fixed with one end of the cylinder. Through the other end of the cylinder, the plastic tubes were taken out in order to connect them with the inclined multi-manometer. This end was supported in the groove of the sidewall of the extended portion, compatible with the pentagonal and hexagonal end of the cylinder. The capillary tube made of copper was used to make the tapping on the sides of the square, pentagonal and hexagonal model cylinders. These copper tubes were connected with the plastic tubes. The cylinder was leveled and then fixed very carefully so that its top side was parallel to the flow direction.

There was a provision for rotation of the test cylinder at various angles to obtain the wind load at different angles of attack. The Reynolds number was 4.89×10^4 based on the projected width of the cylinder across the flow direction. Since the top and bottom of the extended part of the wind tunnel was open; as such no correction for blockage was done in the analysis. The test cylinders were placed very close to the end of the wind tunnel so that the approach velocity on the test cylinders was approximately identical as that in the exit end of the wind tunnel. The provision was also kept in the extended wall to fix the pentagonal and hexagonal cylinders and one square cylinder along the flow direction. There was also a scope to change the inter-spacing between the cylinders.

The cylinders were fixed at one end by the help of bolt and nut and the other ends were fixed in groove. Through the grooves the plastic tubes were taken out and connected with the inclined multi-manometer as in the single cylinder. During fixing the cylinders, it was carefully checked whether the top side of the cylinders were parallel to the free stream velocity direction. Leveling of the test cylinder was always checked by a standard spirit level.

3.4 Construction of the Cylinders

For the study, one square, one hexagonal cylinder and one pentagonal cylinder of identical size were constructed. Each of the cylinders was made of seasoned teak wood in order to avoid the bucking and expansion due to the change of temperature and humidity. The tapping positions on the cross-section of the cylinder are shown in Figure 3.3. The projected width (D) of the square, hexagonal and pentagonal cylinder was 50 mm. Each face of the cylinder contained five tappings on each side. The distance between the consecutive tapping points was equal (Δd) as shown in the figure. However, the location of the corner tapping was at a distance of $\frac{1}{2}(\Delta d)$.

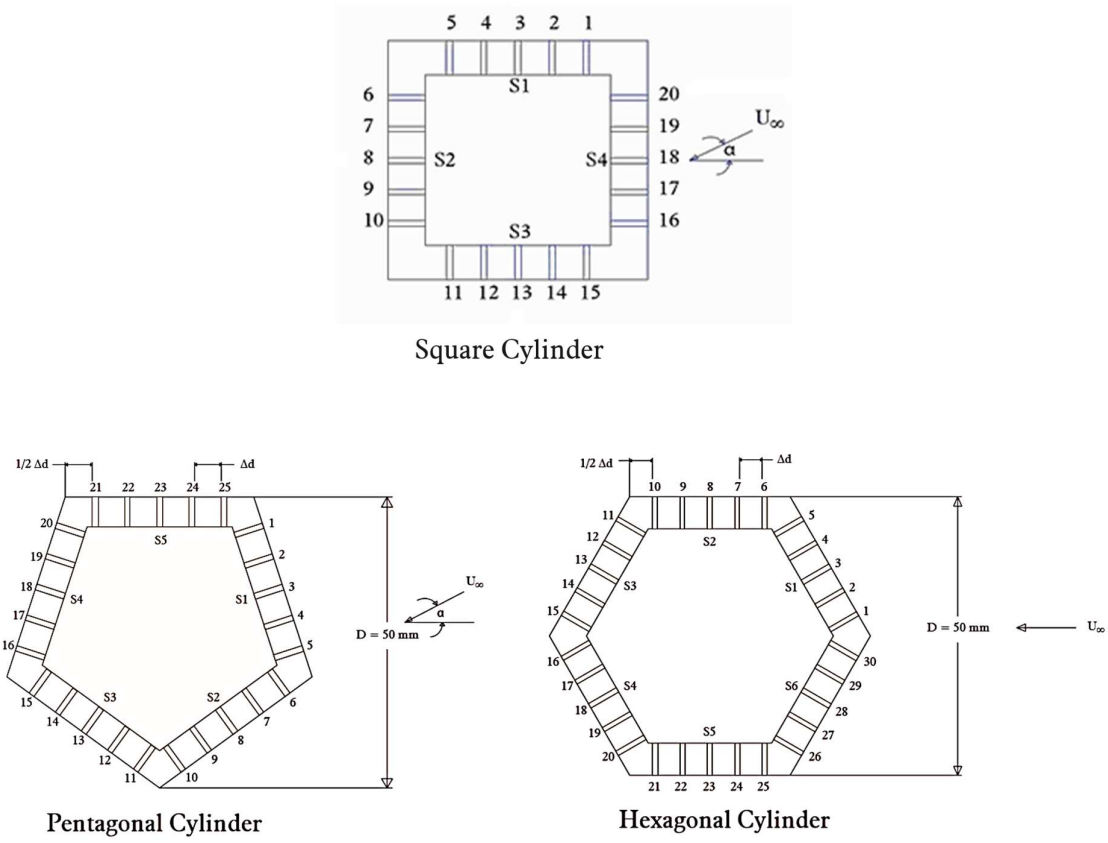

Figure 3. 3: Tapping positions shown on cross-section of cylinders

Each tapping was identified by a numerical number from 1 to 20 for square cylinder, from 1 to 30 for hexagonal cylinder and from 1 to 25 for pentagonal cylinder as can be seen from the figure. The tappings were not made along the cross-section of the cylinder. They were located within some span of the cylinder. To avoid manufacturing problem this technique was followed. Since the velocity was two-dimensional flow, this would not make any effect on

the experimental result. On one side of the cylinder a steel plate was attached through which there was a bolt for fixing the cylinder with the side wall of the extended tunnel. The other side of the cylinder was hollow through which the plastic tubes were allowed to pass. The plastic tubes were connected with the copper capillary tubes at one side and at the other side with the inclined multi-manometer. The manometer liquid was water. The tappings were made of copper tubes of 1.71 mm outside diameter. Each tapping was of 10 mm length approximately. From the end of the copper tube flexible plastic tube of 1.70 mm inner diameter was press fitted.

3.5 Arrangement of Cylinders

In the experimental investigation, one square, one pentagonal and one hexagonal cylinder were used, where square cylinder was in the downstream side having one pentagonal and one hexagonal cylinder in the upstream side in a uniform cross flow. The square cylinder was placed centrally along the flow direction.

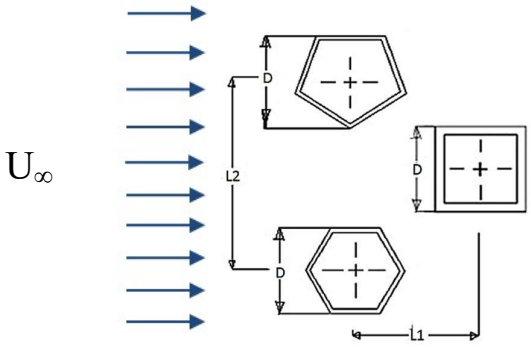

Figure 3. 4: Tunnel test section showing position of group cylinders

In Figure 3.4 the position of the group of cylinders at zero angle of attack is shown in the wind tunnel test section. The inter-spacing between upstream (pentagonal and hexagonal) and downstream (square) cylinders was taken as $L_1 = 1D$ i.e. 50 mm and between two upstream cylinders were taken as $L_2 = 2D$.

3.6 Measuring Equipment

The wind velocity across the test section of the wind tunnel was measured with the help of digital anemometer. A pitot tube was also used to measure the velocity in order to cross check. The pitot tube was connected to an inclined manometer the limb of which contained water. The surface static pressures were measured with the help of inclined manometer. The inclination of the manometer was sufficient to record the pressure with reasonable accuracy.

CHAPTER-4

MATHEMATICAL MODEL AND SIMULATION

4.1 General

The calculation procedure of finding pressure coefficients, drag and lift coefficients has been described briefly in this chapter along with the simulation procedure. From the measured surface static pressure on the square, pentagonal and hexagonal cylinders the pressure coefficients are obtained. Then the drag and lift coefficients are found from the pressure coefficients. With the help of numerical integration method drag and lift coefficients are determined experimentally.

4.2 Determination of Pressure Coefficient

The pressure coefficient is defined as

$$C_P = \frac{\Delta P}{\frac{1}{2}\rho U_\infty^2} \tag{4.1}$$

where, $\Delta P = P - P_0$

P is the static pressure on the surface of the cylinder, P_0 is the ambient pressure, ρ is the density of the air, U_∞ is the free stream velocity.

ΔP is obtained from

$$\Delta P = \Delta h_w \times \gamma_w \tag{4.2}$$

where, Δh_w is the manometer reading and γ_w is the specific weight of manometer liquid (H_2O).

Figure 4.1 shows the section of the model square, pentagonal and hexagonal cylinders with the pressure tapping points, at each of which the static pressure was recorded with the help of inclined multi-manometer. The cylinders were rotated at various angles of 0^0, 30^0, 45^0, 60^0 and at each angle surface static pressures were recorded with the help of multi-manometer.

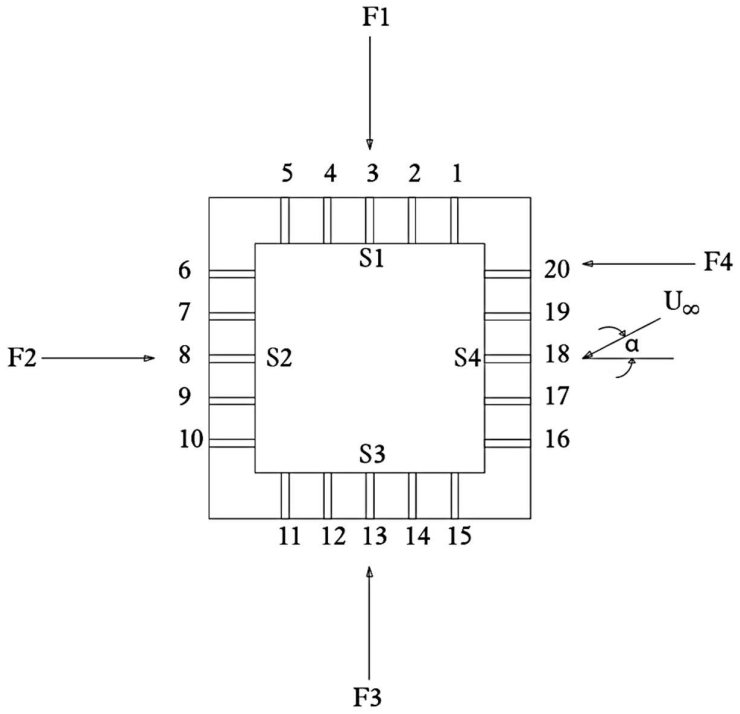

Square Cylinder

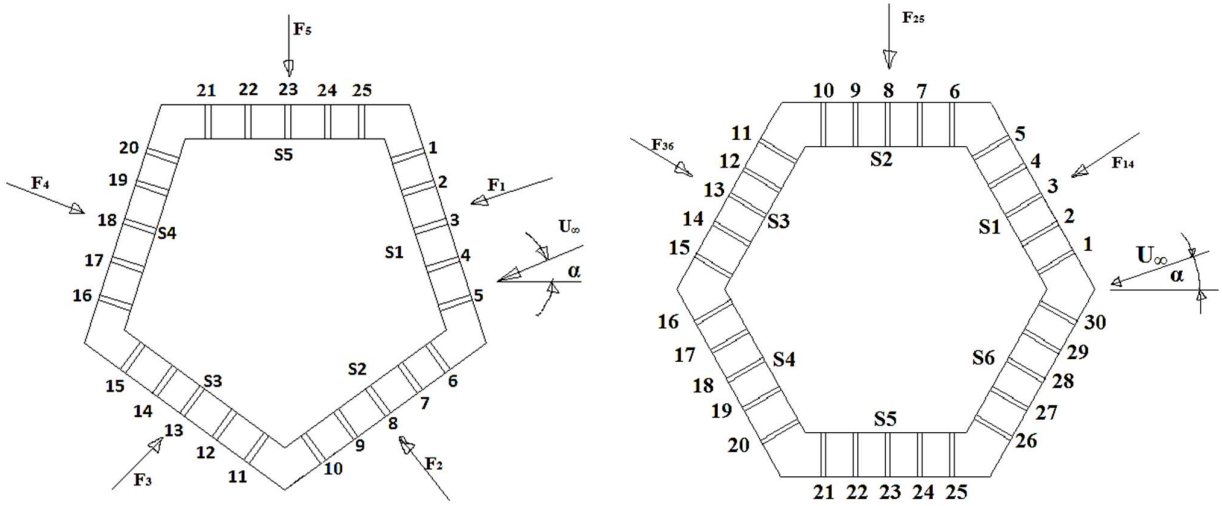

Pentagonal Cylinder

Hexagonal Cylinder

Figure 4. 1: Cross-section of Cylinders Showing Forces

4.3 Determination of Drag and Lift Coefficients

Drag and lift coefficients for different types of cylinder are calculated here with the help of numerical integration method.

4.3.1 Square Cylinder

As shown in Figure 4.1 that the cylinder has four faces S_1, S_2, S_3, and S_4. The pressure differences between the various tapping points along the face S_2 and S_4 (horizontal forces) can be obtained from

$\Delta P_{6-20} = P_6 - P_{20}$ is the pressure difference between tapping points 6 and 20

$\Delta P_{7-19} = P_7 - P_{19}$ is the pressure difference between tapping points 7 and 19

$\Delta P_{8-18} = P_8 - P_{18}$ is the pressure difference between tapping points 8 and 18

$\Delta P_{9-17} = P_9 - P_{17}$ is the pressure difference between tapping points 9 and 17

$\Delta P_{10-16} = P_{10} - P_{16}$ is the pressure difference between tapping points 10 and 16

Now, to calculate F_D and C_D,

$$F_D = \left(\frac{\Delta P_{1h} \times \gamma_w \times \Delta l \times 1}{10} + \frac{\Delta P_{2h} \times \gamma_w \times \Delta l \times 1}{10} + \frac{\Delta P_{3h} \times \gamma_w \times \Delta l \times 1}{10} + \frac{\Delta P_{4h} \times \gamma_w \times \Delta l \times 1}{10} + \frac{\Delta P_{5h} \times \gamma_w \times \Delta l \times 1}{10} \right) \times \cos\alpha +$$

$$\left(\frac{\Delta P_{1v} \times \gamma_w \times \Delta l \times 1}{10} + \frac{\Delta P_{2v} \times \gamma_w \times \Delta l \times 1}{10} + \frac{\Delta P_{3v} \times \gamma_w \times \Delta l \times 1}{10} + \frac{\Delta P_{4v} \times \gamma_w \times \Delta l \times 1}{10} + \frac{\Delta P_{5v} \times \gamma_w \times \Delta l \times 1}{10} \right) \times \sin\alpha$$

$$= \frac{\gamma_w \times \Delta l \times 1}{10} \left[\left(\Delta P_{1h} + \Delta P_{2h} + \Delta P_{3h} + \Delta P_{4h} + \Delta P_{5h} \right) \cos\alpha + \left(\Delta P_{1v} + \Delta P_{2v} + \Delta P_{3v} + \Delta P_{4v} + \Delta P_{5v} \right) \sin\alpha \right]$$

$$= \frac{\gamma_w \times \Delta l \times 1}{10} \left(\Delta P_D \right)$$

$$C_D = \frac{\gamma_w \times \Delta l \times 1 \times \Delta P_D}{10 \times \frac{1}{2} \times \rho \times A \times U_\infty^2} = \frac{\gamma_w \times \Delta P_D}{25 \rho U_\infty^2}$$

$$C_D = \gamma_w \left[\left(\Delta P_{1h} + \Delta P_{2h} + \Delta P_{3h} + \Delta P_{4h} + \Delta P_{5h} \right) \cos\alpha + \left(\Delta P_{1v} + \Delta P_{2v} + \Delta P_{3v} + \Delta P_{4v} + \Delta P_{5v} \right) \sin\alpha \right] \times \frac{1}{25 \rho U_\infty^2}$$

$$= \frac{\gamma_w\left[\left(P_6 - P_{20} + P_7 - P_{19} + P_8 - P_{18} + P_9 - P_{17} + + P_{10} - P_{16}\right)\cos\alpha\right]}{25\rho\mu_0^2} +$$

$$\frac{\gamma_w\left[\left(P_{11-} P_5 + P_{12} - P_4 + P_{13} - P_3 + P_{14} - P_2 + P_{15} - P_1\right)\sin\alpha\right]}{25\rho U_\infty^2}$$

$$F_L = \frac{\gamma_w \times \Delta l \times 1}{10}\left(\Delta P_h \sin\alpha + \Delta P_v \cos\alpha\right)$$

$$C_L = \frac{\gamma_w \times \Delta P_L}{25 \times \rho \times U_\infty^2} =$$

$$\gamma_w\left[\left(\Delta P_{1h} + \Delta P_{2h} + \Delta P_{3h} + \Delta P_{4h} + \Delta P_{5h}\right)\sin\alpha + \left(\Delta P_{1v} + \Delta P_{2v} + \Delta P_{3v} + \Delta P_{4v} + \Delta P_{5v}\right)\cos\alpha\right] \times \frac{1}{25\rho U_\infty^2}$$

4.3.2 Hexagonal Cylinder

As shown in Figure 4.1 that the cylinder has six faces S_1, S_2, S_3, S_4, S_5 and S_6. The pressure differences between the various tapping points along the face S_1 and S_4 can be obtained from

$\Delta P_{1-20} = P_1 - P_{20}$ is the pressure difference between tapping points 1 and 20

$\Delta P_{2-1} = P_2 - P_{19}$ is the pressure difference between tapping points 2 and 19

$\Delta P_{3-18} = P_3 - P_{18}$ is the pressure difference between tapping points 3 and 18

$\Delta P_{4-17} = P_4 - P_{17}$ is the pressure difference between tapping points 4 and 17

$\Delta P_{5-16} = P_5 - P_{16}$ is the pressure difference between tapping points 5 and 16

If F_{14} indicates the net force along the faces S_1 and S_4, then using Simpson's rule, one can find

$$F_{14} = \frac{\Delta A}{3}[\Delta P_{1\text{-}20} + 4\Delta P_{2\text{-}19} + 2\Delta P_{3\text{-}18} + 4\Delta P_{4\text{-}17} + \Delta P_{5\text{-}16}] \quad (4.3)$$

If the length of the cylinder is chosen as unity, then the above expression becomes

$$F_{14} = \frac{\Delta d \; x \; 1}{3}[\Delta P_{1\text{-}20} + 4\Delta P_{2\text{-}19} + 2\Delta P_{3\text{-}18} + 4\Delta P_{4\text{-}17} + \Delta P_{5\text{-}16}]$$

$$= \frac{\Delta d}{3}[(P_1 - P_{20}) + 4(P_2 - P_{19}) + 2(P_3 - P_{18}) + 4(P_4 - P_{17}) + (P_5 - P_{16})]$$

$$= \frac{\Delta d}{3}[(P_1 - P_0) - (P_{20} - P_0) + 4(P_2 - P_0) - 4(P_{19} - P_0) + 2(P_3 - P_0) - 2(P_{18} - P_0)$$

$$+4(P_4 - P_0) - 4(P_{17} - P_0) + (P_5 - P_0) - (P_{16} - P_0)] \quad (4.4)$$

If the component of the force $F_{d_{14}}$ occurs along the flow direction, then one can find the expression of F as $F_{d_{14}}$

$$F_{d_{14}} = F_{14}\, cos(\,30^0 - \alpha) \tag{4.5}$$

Similarly the force component $F_{L_{14}}$ in a direction perpendicular to the flow may be written as

$$F_{L_{14}} = -F_{14}\, sin(30^0 - \alpha) \tag{4.6}$$

The net force F_{25} along the faces S_2 and S_5 can be obtained in the same way as above and that is

$$F_{25} = \frac{\Delta d}{3}[(P_6 - P_0) - (P_{25} - P_0) + 4(P_7 - P_0) - 4(P_{24} - P_0) + 2(P_8 - P_0) - 2(P_{23} - P_0)$$

$$+4(P_9 - P_0) - 4(P_{22} - P_0) + (P_{10} - P_0) - (P_{21} - P_0)] \tag{4.7}$$

Therefore, the components of the drag and lift forces along the faces S_2 and S_5 are respectively

$$F_{d_{25}} = F_{25}\, cos(\,90^0 - \alpha) \tag{4.8}$$

$$F_{L_{25}} = -F_{25}\, sin(90^0 - \alpha) \tag{4.9}$$

The net force F_{36} along the faces S_3 and S_6 can be obtained in the same way as above and that is

$$F_{36} = \frac{\Delta d}{3}[(P_{11} - P_0) - (P_{30} - P_0) + 4(P_{12} - P_0) - 4(P_{29} - P_0) + 2(P_{13} - P_0) - 2(P_{28} - P_0)$$

$$+4(P_{14} - P_0) - 4(P_{27} - P_0) + (P_{15} - P_0) - (P_{26} - P_0)] \tag{4.10}$$

Therefore, the components of the drag and lift forces along the faces S_3 and S_6 are respectively

$$F_{d_{36}} = F_{36}\, cos(\,150^0 - \alpha) \tag{4.11}$$

$$F_{L_{36}} = -F_{36}\, sin(150^0 - \alpha) \tag{4.12}$$

Drag and lift coefficients are defined as follows

$$C_D = \frac{F_d}{\frac{1}{2}\rho A U_\infty^2} \tag{4.13}$$

and $C_L = \frac{F_L}{\frac{1}{2}\rho A U_\infty^2}$ (4.14)

where, A is the frontal projected area of the cylinder

The total drag force along the flow direction is

$$F_d = F_{d_{14}} + F_{d_{25}} + F_{d_{36}} \quad (4.15)$$

and total lift force in a direction perpendicular to flow is

$$F_L = F_{L_{14}} + F_{L_{25}} + F_{L_{36}} \quad (4.16)$$

Now from equations (4.13) and (4.15), the expression of drag coefficient becomes

$$C_D = \frac{F_{d_{14}} + F_{d_{25}} + F_{d_{36}}}{\frac{1}{2}\rho A U_\infty^2}$$

Now substituting the values of $F_{d_{14}}$, $F_{d_{25}}$ and $F_{d_{36}}$ from equations (4.5), (4.8) and (4.11) respectively, the expression of drag coefficient becomes

$$C_D = \frac{F_{14}\cos(30^0 - \alpha) + F_{25}\cos(90^0 - \alpha) + F_{36}\cos(150^0 - \alpha)}{\frac{1}{2}\rho A U_\infty^2}$$

$$= \frac{\cos(30^0 - \alpha)}{A} \cdot \frac{F_{14}}{\frac{1}{2}\rho U_\infty^2} + \frac{\cos(90^0 - \alpha)}{A} \cdot \frac{F_{25}}{\frac{1}{2}\rho U_\infty^2}$$

$$+ \frac{\cos(150^0 - \alpha)}{A} \frac{F_{36}}{\frac{1}{2}\rho U_\infty^2} \quad (4.17)$$

Now inserting the values of F_{14}, F_{25} and F_{36} from equations (4.4), (4.7) and (4.10) respectively, one finds

$$C_D = \frac{\cos(30^0-\alpha)\times\Delta d}{3A} \cdot \frac{1}{\frac{1}{2}\rho U_\infty^2} \cdot [(P_1 - P_0) - (P_{20} - P_0) + 4(P_2 - P_0) - 4(P_{19} - P_0) + 2(P_3 - P_0) -$$

$$2(P_{18} - P_0) + 4(P_4 - P_0) - 4(P_{17} - P_0) + (P_5 - P_0) - (P_{16} - P_0)] + \frac{\cos(90^0-\alpha)\times\Delta d}{3A} \cdot \frac{1}{\frac{1}{2}\rho U_\infty^2} \cdot [(P_6$$

$$- P_0) - (P_{25} - P_0) + 4(P_7 - P_0) - 4(P_{24} - P_0) + 2(P_8 - P_0) - 2(P_{23} - P_0) + 4(P_9 - P_0) - 4(P_{22} -$$

$$P_0) + (P_{10} - P_0) - (P_{21} - P_0)] + \frac{\cos(150^0-\alpha)\times\Delta d}{3A} \cdot \frac{1}{\frac{1}{2}\rho U_\infty^2} \cdot [(P_{11} - P_0) - (P_{30} - P_0) + 4(P_{12} - P_0)$$

$-4(P_{29}-P_0)+2(P_{13}-P_0)-2(P_{28}-P_0)+4(P_{14}-P_0)-4(P_{27}-P_0)+(P_{15}-P_0)-(P_{26}-P_0)]$

Now writing in terms of pressure coefficients the above equation is transformed into

$$C_D=\frac{cos(30^0-\alpha)\times\Delta d}{3A}\cdot[C_{p_1}-C_{p_{20}}+4C_{p_2}-4C_{p_{19}}+2C_{p_3}-2C_{p_{18}}+4C_{p_4}-4C_{p_{17}}+C_{p_5}-C_{p_{16}}]$$
$$+\frac{cos(90^0-\alpha)\times\Delta d}{3A}\cdot[C_{p_6}-C_{p_{25}}+4C_{p_7}-4C_{p_{24}}+2C_{p_8}-2C_{p_{23}}+4C_{P_9}-4C_{p_{22}}+C_{p_{10}}-C_{p_{26}}]+$$
$$\frac{cos(135^0-\alpha)\times\Delta d}{3A}\cdot[C_{p_{11}}-C_{p_{30}}+4C_{p_{12}}-4C_{p_{29}}+2C_{p_{13}}-2C_{p_{28}}+4C_{p_{14}}-4C_{p_{27}}+C_{p_{15}}-C_{p_{26}}]$$

Now rearranging the expression of C_D becomes of the following form

$$C_D=\frac{cos(30^0-\alpha)\times\Delta d}{3A}\cdot[(C_{p_1}+4C_{p_2}+2C_{p_3}+4C_{p_4}+C_{p_5})-(C_{p_{16}}+4C_{p_{17}}+2C_{p_{18}}+4C_{p_{19}}+$$
$$C_{p_{20}})]+\frac{cos(90^0-\alpha)\times\Delta d}{3A}\cdot[(C_{p_6}+4C_{p_7}+2C_{p_8}+4C_{P_9}+C_{p_{10}})-$$
$$(C_{p_{21}}+4C_{p_{22}}+2C_{p_{23}}+4C_{p_{24}}+$$
$$C_{p_{25}})+\frac{cos(150^0-\alpha)\times\Delta d}{3A}\cdot[(C_{p_{11}}+4C_{p_{12}}+2C_{p_{13}}+4C_{p_{14}}+C_{p_{15}})-(C_{p_{26}}+4C_{p_{27}}+2C_{p_{28}}+$$
$$4C_{p_{29}}+C_{p_{30}})] \quad (4.18)$$

Similarly, the expression of lift coefficient C_L can be obtained as,

$$C_L=-\frac{sin(30^0-\alpha)\times\Delta d}{3A}\cdot[(C_{p_1}+4C_{p_2}+2C_{p_3}+4C_{p_4}+C_{p_5})-(C_{p_{16}}+4C_{p_{17}}+2C_{p_{18}}+4C_{p_{19}}+$$
$$C_{p_{20}})]-\frac{sin(90^0-\alpha)\times\Delta d}{3A}\cdot[(C_{p_6}+4C_{p_7}+2C_{p_8}+4C_{P_9}+C_{p_{10}})-(C_{p_{21}}+4C_{p_{22}}+2C_{p_{23}}+4C_{p_{24}}+$$
$$C_{p_{25}})]-\frac{sin(150^0-\alpha)\times\Delta d}{3A}\cdot[(C_{p_{11}}+4C_{p_{12}}+2C_{p_{13}}+4C_{p_{14}}+C_{p_{15}})-(C_{p_{26}}+4C_{p_{27}}+2C_{p_{28}}+$$
$$4C_{p_{29}}+C_{p_{30}})] \quad (4.19)$$

4.3.3 Pentagonal Cylinder

As shown in Figure 4.1, the cylinder has five faces S_1, S_2, S_3, S_4 and S_5. The pressure at the various tapping points along the face S_1 can be written as,

$P_1, \ldots, P_5 =$ Pressure at tapping point 1 to 5.

If F_1 indicates the force along the faces S_1, then using Simpson's rule, one can find

$$F_1=\frac{\Delta A}{3}[P_1+4P_2+2P_3+4P_4+P_5]$$

If the length of the cylinder is chosen as unity, then the above expression becomes

$$F_1 = \frac{\Delta d \, x \, 1}{3}[\, P_1 \, + 4P_2 + 2P_3 + \, 4P_4 + \, P_5]$$

$$= \frac{\Delta d}{3}[(P_1 - P_0) + 4(P_2 - P_0) + 2(P_3 - P_0) + 4(P_4 - P_0) + (P_5 - P_0) + 12P_0] \quad (4.20)$$

If the component of the force F_{d_1} occurs along the flow direction, then one can find the expression of F as F_{d_1}

$$F_{d_1} = F_1 \cos(18^0 - \alpha) \quad (4.21)$$

Similarly the force component F_{L_1} in a direction perpendicular to the flow, may be written as

$$F_{L_1} = -F_1 \sin(18^0 - \alpha) \quad (4.22)$$

The net force F_2 along the face S_2 can be obtained in the same way as above and that is

$$F_2 = \frac{\Delta d}{3}[(P_6 - P_0) + 4(P_7 - P_0) + 2(P_8 - P_0) + 4(P_9 - P_0) + (P_{10} - P_0) + 12\, P_0] \quad (4.23)$$

Therefore, the components of the drag and lift forces along the face S_2 are respectively

$$F_{d_2} = -F_2 \cos(126^0 - \alpha) \quad (4.24)$$

$$F_{L_2} = F_2 \sin(126^0 - \alpha) \quad (4.25)$$

The net force F_3 along the face S_3 can be obtained in the same way as above and that is

$$F_3 = \frac{\Delta d}{3}[(P_{11} - P_0) + 4(P_{12} - P_0) + 2(P_{13} - P_0) + 4(P_{14} - P_0) + (P_{15} - P_0) + 12\, P_0 \quad (4.26)$$

Therefore, the components of the drag and lift forces along the face S_3 are respectively

$$F_{d_3} = -F_3 \cos(54^0 - \alpha) \quad (4.27)$$

$$F_{L_3} = F_3 \sin(54^0 - \alpha) \quad (4.28)$$

The net force F_4 along the face S_4 can be obtained in the same way as above and that is

$$F_4 = \frac{\Delta d}{3}[(P_{16} - P_0) + 4(P_{17} - P_0) + 2(P_{18} - P_0) + 4(P_{19} - P_0) + (P_{20} - P_0) + 12P_0] \quad (4.29)$$

Therefore, the components of the drag and lift forces along the face S_4 are respectively

$$F_{d_4} = F_4 \cos(162^0 - \alpha) \tag{4.30}$$

$$F_{L_4} = -F_4 \sin(162^0 - \alpha) \tag{4.31}$$

The net force F_5 along the face S_5 can be obtained in the same way as above and that is

$$F_5 = \frac{\Delta d}{3}[(P_{21} - P_0) + 4(P_{22} - P_0) + 2(P_{23} - P_0) + 4(P_{24} - P_0) + (P_{25} - P_0) + 12P_0] \tag{4.32}$$

Therefore, the components of the drag and lift forces along the face S_5 are respectively

$$F_{d_5} = F_5 \cos(90^0 - \alpha) \tag{4.33}$$

$$F_{L_5} = -F_5 \sin(90^0 - \alpha) \tag{4.34}$$

Drag and lift coefficients are defined as follows

$$C_D = \frac{F_d}{\frac{1}{2}\rho A U_\infty^2} \tag{4.35}$$

$$C_L = \frac{F_L}{\frac{1}{2}\rho A U_\infty^2} \tag{4.36}$$

where, A is the frontal area of the cylinder

The total drag force along the flow direction is

$$F_d = F_{d_1} + F_{d_2} + F_{d_3} + F_{d_4} + F_{d_5} \tag{4.37}$$

and total lift force in a direction perpendicular to flow is

$$F_L = F_{L_1} + F_{L_2} + F_{L_3} + F_{L_4} + F_{L_5} \tag{4.38}$$

Now from equations (4.35) and (4.37), the expression of drag coefficient becomes

$$C_D = \frac{F_{d_1} + F_{d_2} + F_{d_3} + F_{d_4} + F_{d_5}}{\frac{1}{2}\rho A U_\infty^2}$$

Now substituting the values of F_{d_1}, F_{d_2}, F_{d_3}, F_{d_4} and F_{d_5} from equations (4.21), (4.24), (4.27), (4.30) and (4.33) respectively, the expression of drag coefficient becomes

$$C_D = \frac{F_1 \cos(18^0 - \alpha) - F_2 \cos(126^0 - \alpha) - F_3 \cos(54^0 - \alpha) + F_4 \cos(162^0 - \alpha) + F_5 \cos(90^0 - \alpha)}{\frac{1}{2}\rho A U_\infty^2}$$

$$= \frac{\cos(18^0 - \alpha)}{A} \cdot \frac{F_1}{\frac{1}{2}\rho U_\infty^2} - \frac{\cos(126^0 - \alpha)}{A} \cdot \frac{F_2}{\frac{1}{2}\rho U_\infty^2} - \frac{\cos(54^0 - \alpha)}{A} \cdot \frac{F_3}{\frac{1}{2}\rho U_\infty^2} + \frac{\cos(162^0 - \alpha)}{A} \cdot \frac{F_4}{\frac{1}{2}\rho U_\infty^2} + \frac{\cos(90^0 - \alpha)}{A} \cdot \frac{F_5}{\frac{1}{2}\rho U_\infty} \quad (4.39)$$

Now inserting the values of F_1, F_2, F_3, F_4 and F_5 from equations (4.20), (4.23), (4.26), (4.29) and (4.32) respectively, one finds

$$C_D = \frac{\cos(18^0-\alpha)\times\Delta d}{3A} \cdot \frac{1}{\frac{1}{2}\rho U_\infty^2} \cdot [(P_1 - P_0) + 4(P_2 - P_0) + 2(P_3 - P_0) + 4(P_4 - P_0) + (P_5 - P_0) + 12P_0] - \frac{\cos(126^0-\alpha)\times\Delta d}{3A} \cdot \frac{1}{\frac{1}{2}\rho U_\infty^2} \cdot [(P_6 - P_0) + 4(P_7 - P_0) + 2(P_8 - P_0) + 4(P_9 - P_0) + (P_{10} - P_0) + 12P_0] - \frac{\cos(54^0-\alpha)\times\Delta d}{3A} \cdot \frac{1}{\frac{1}{2}\rho U_\infty^2} \cdot [(P_{11} - P_0) + 4(P_{12} - P_0) + 2(P_{13} - P_0) + 4(P_{14} - P_0) + (P_{15} - P_0) + 12P_0] + \frac{\cos(162^0-\alpha)\times\Delta d}{3A} \cdot \frac{1}{\frac{1}{2}\rho U_\infty^2} \cdot [(P_{16} - P_0) + 4(P_{17} - P_0) + 2(P_{18} - P_0) + 4(P_{19} - P_0) + (P_{20} - P_0) + 12P_0] + \frac{\cos(90^0-\alpha)\times\Delta d}{3A} \cdot \frac{1}{\frac{1}{2}\rho U_\infty^2} \cdot [(P_{21} - P_0) + 4(P_{22} - P_0) + 2(P_{23} - P_0) + 4(P_{24} - P_0) + (P_{25} - P_0) + 12P_0]$$

Now writing in terms of pressure coefficients and using $12P_0 = 0$ [P_0 is the ambient gauge pressure = 0] the above equation is transformed into

$$C_D = \frac{\cos(18^0-\alpha)\times\Delta d}{3A} \cdot [C_{p_1} + 4C_{p_2} + 2C_{p_3} + 4C_{p_4} + C_{p_5}] - \frac{\cos(126^0-\alpha)\times\Delta d}{3A} \cdot [C_{p_6} + 4C_{p_7} + 2C_{p_8} + 4C_{P_9} + C_{p_{10}}] - \frac{\cos(54^0-\alpha)\times\Delta d}{3A} \cdot [C_{p_{11}} + 4C_{p_{12}} + 2C_{p_{13}} + 4C_{p_{14}} + C_{p_{15}}] + \frac{\cos(162^0-\alpha)\times\Delta d}{3A} \cdot [C_{p_{16}} + 4C_{p_{17}} + 2C_{p_{18}} + 4C_{p_{19}} + C_{p_{20}}] + \frac{\cos(90^0-\alpha)\times\Delta d}{3A} \cdot [C_{p_{21}} + 4C_{p_{22}} + 2C_{p_{23}} + 4C_{p_{24}} + C_{p_{25}}] \quad (4.40)$$

Similarly, the expression of lift coefficient C_L can be obtained as,

$$C_L = -\frac{sin(18^0-\alpha)\times\Delta d}{3A}\cdot[C_{p_1}+4C_{p_2}+2C_{p_3}+4C_{p_4}+C_{p_5}] + \frac{sin(126^0-\alpha)\times\Delta d}{3A}\cdot[C_{p_6}+4C_{p_7}+ 2C_{p_8}+4C_{P_9}+C_{p_{10}}] + \frac{sin(54^0-\alpha)\times\Delta d}{3A}\cdot[C_{p_{11}}+4C_{p_{12}}+2C_{p_{13}}+4C_{p_{14}}+C_{p_{15}}] - \frac{sin(162^0-\alpha)\times\Delta d}{3A}\cdot[C_{p_{16}}+4C_{p_{17}}+2C_{p_{18}}+4C_{p_{19}}+C_{p_{20}}] - \frac{sin(90^0-\alpha)\times\Delta d}{3A}\cdot[C_{p_{21}}+4C_{p_{22}}+2C_{p_{23}} + 4C_{p_{24}}+C_{p_{25}}] \quad (4.41)$$

4.4 Mathematical Formulation and Turbulence Model

Navier-Stokes equations are the combination of continuity, momentum and energy equations. The solver used for the computational analysis actually solve these equations for any kind of flow. But in case of turbulent flows, additional transport equations are also need to be solved by the solver. Regarding wind flow around the different shape of cylinders, the governing equations can be represented by Reynolds-averaged Navier Stokes (RANS) equations as follows:

$$\frac{\partial u_i}{\partial x_i} = 0 \quad (4.42)$$

$$\frac{\partial}{\partial x_j}(\rho u_j u_i) = -\frac{\partial p}{\partial x_j} + \frac{\partial}{\partial x_j}[\mu(\frac{\partial u_i}{\partial x_j}+\frac{\partial u_j}{\partial x_i}) - \rho\overline{u_i' u_j'}] \quad (4.43)$$

To solve the additional quantities due to turbulent flow, K-epsilon (k-ε) turbulence model is used which is the most common model used in Computational Fluid Dynamics (CFD) to simulate mean flow characteristics for turbulent flow conditions. It is a two equation model which gives a general description of turbulence by means of two transport equations (PDEs). This model uses Boussinesq hypothesis to relate the Reynolds stresses to the mean velocity gradients. The Boussinesq hypothesis is also used in the Spalart-Allmaras and the k- ω models. In k-epsilon model, two additional transport equations that is for the turbulence kinetic energy, *k*, and the turbulence dissipation rate, *ε* are solved as shown on the screen. But in other model only one transport equation is solved which represents turbulent viscosity, which is not suitable for the flow type involved in this work.

The exact k-ε equations contain many unknown and unmeasurable terms. For a much more practical approach, the standard k-ε turbulence model (Launder and Spalding, 1974) is used which is based on our best understanding of the relevant processes, thus minimizing unknowns and presenting a set of equations which can be applied to a large number of turbulent applications.

For turbulent kinetic energy, k

$$\frac{\partial(\rho k)}{\partial t} + \frac{\partial(\rho k u_i)}{\partial x_i} = \frac{\partial}{\partial x_j}\left[\frac{\mu_t}{\sigma_k}\frac{\partial k}{\partial x_j}\right] + 2\mu_t E_{ij}E_{ij} - \rho\epsilon \tag{4.44}$$

For turbulence dissipation rate, ε

$$\frac{\partial(\rho\epsilon)}{\partial t} + \frac{\partial(\rho\epsilon u_i)}{\partial x_i} = \frac{\partial}{\partial x_j}\left[\frac{\mu_t}{\sigma_\epsilon}\frac{\partial \epsilon}{\partial x_j}\right] + C_{1\epsilon}\frac{\epsilon}{k}2\mu_t E_{ij}E_{ij} - C_{2\epsilon}\rho\frac{\epsilon^2}{k} \tag{4.45}$$

Rate of change of k or ε + Transport of k or ε by convection = Transport of k or ε by diffusion + Rate of production of k or ε - Rate of destruction of k or ε

where, u_i represents velocity component in corresponding direction

E_{ij} represents component of rate of deformation

μ_t represents eddy viscosity and $\mu_t = \rho C_\mu \frac{K^2}{\varepsilon}$

The equations also consist of some adjustable constants σ_k, σ_ε, $C_{1\varepsilon}$, $C_{2\varepsilon}$. The values of these constants have been arrived at by numerous iterations of data fitting for a wide range of turbulent flows.

4.5 Geometrical Setup

Three different shape of cylinders are used in staggered form for this analysis. Hexagonal and Pentagonal shapes are in upstream position and Square shape is in downstream position. ANSYS 16 is used for geometrical design as well as solver purpose. Numerical results are highly influenced by the dimensions of the geometrical domain. Those are upstream distance (distance between inlet and object), downstream distance (distance between object and outlet), height and width of the domain. The dimensions of the computational flow domain for the simulation purpose is shown in Figure 4.2.

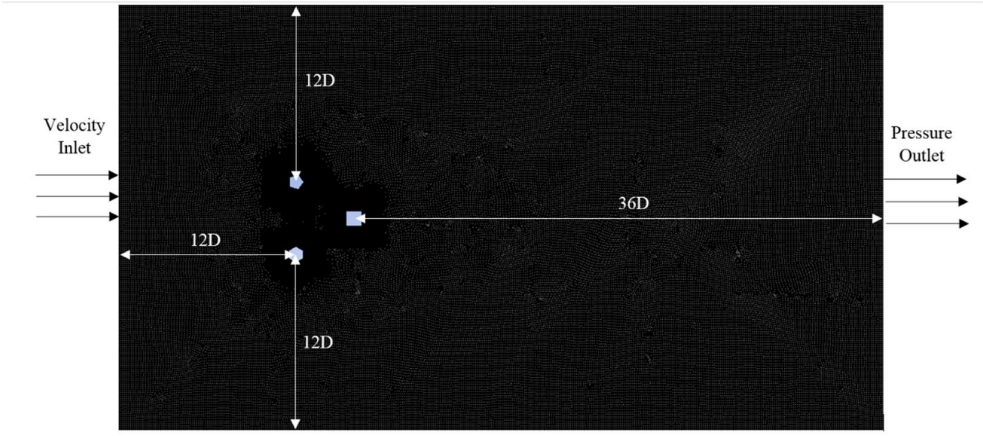

Figure 4. 2: Dimensions of computational flow domain.

4.6 Meshing and Computational Method

An unstructured meshing as shown in figure 4.3 was done consisting of tetrahedron elements. The resolution of meshing was greater in regions where greater computational accuracy was needed like as at the faces of the cylinders. Turbulent flow is assumed and the free stream temperature is *300 K*, which is the same as the environmental temperature. The density of the air at the room temperature is $\rho=1.117\ kg/m^3$ and the viscosity is $\mu=1.86\times10^{-5}\ kg/ms$. Calculations are done for angle of attack of 0˚, 30˚, 45˚, 60˚.

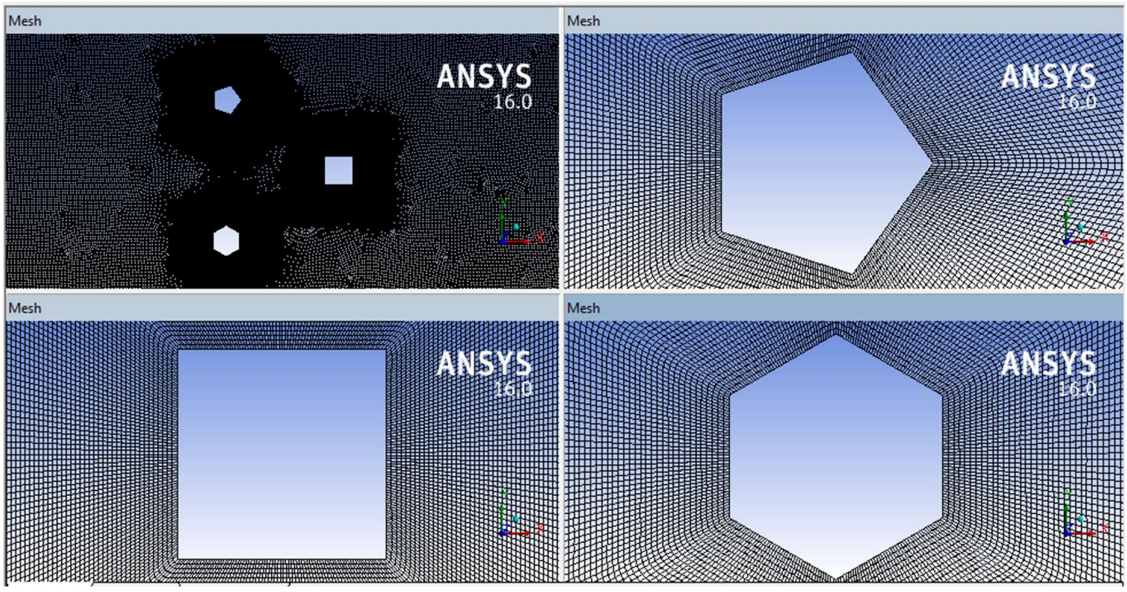

(a) AOA of 0˚

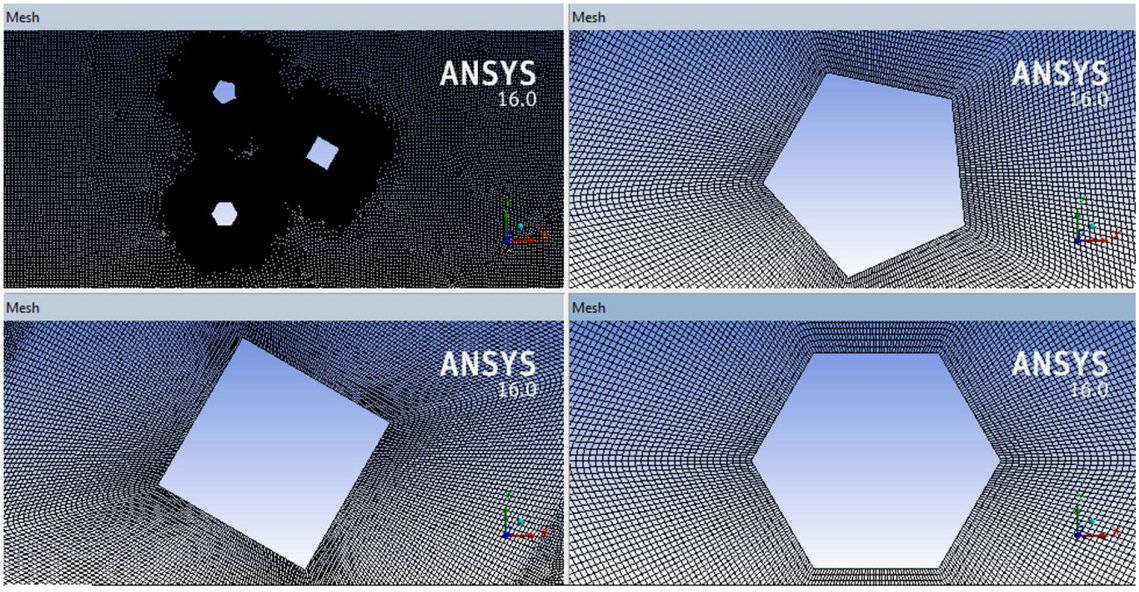

(b) AOA of 30˚

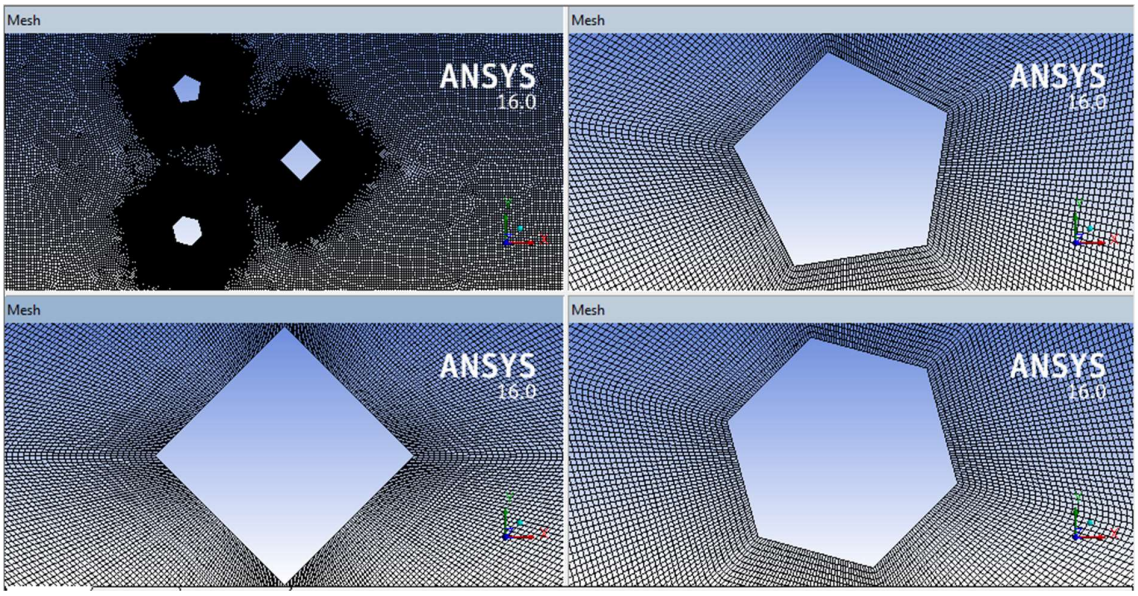

(c) AOA of 45˚

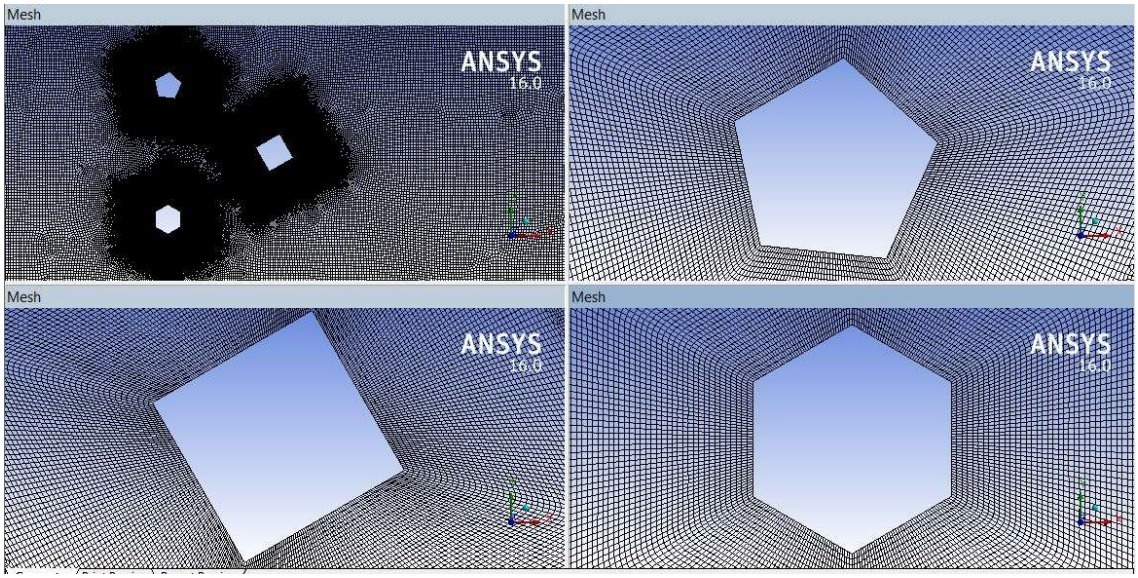

(d) AOA of 60˚

Figure 4. 3: (a) Mesh around the different cylinders at AOA of 0˚, (b) Mesh around the different cylinders at AOA of 30˚, (c) Mesh around the different cylinders at AOA of 45˚, (d) Mesh around the different cylinders at AOA of 60˚

The pre requisite before performing any computational solution is to investigate the effect of mesh size/ number of grid cells on numerical results. Table 4.1 shows the relevant data of meshing.

Table 4. 1: **Mesh Data, Sizing and Quality**

Type of cell	Quadrilateral
Nodes	408047
Minimum Orthogonal Quality	4.65849×10^{-1}
Maximum Ortho Skew	5.34151×10^{-1}
Maximum Aspect Ratio	4.73825

As the mesh size increases, the numerical solution provides more accurate results. But with the additional grid cells, requires more computer memory and computational time. Therefore, an analysis is done with drag co-efficient vs number of nodes, as represented in Figure 4.4. Finer mesh (408047 nodes) is compared with a coarse mesh (190940 nodes) with the same

input. The drag co-efficient of the pentagonal, hexagonal and square cylinders varies by 0.0546%, 0.0022% and 0.0037%, respectively, which is concurrent to the independency test.

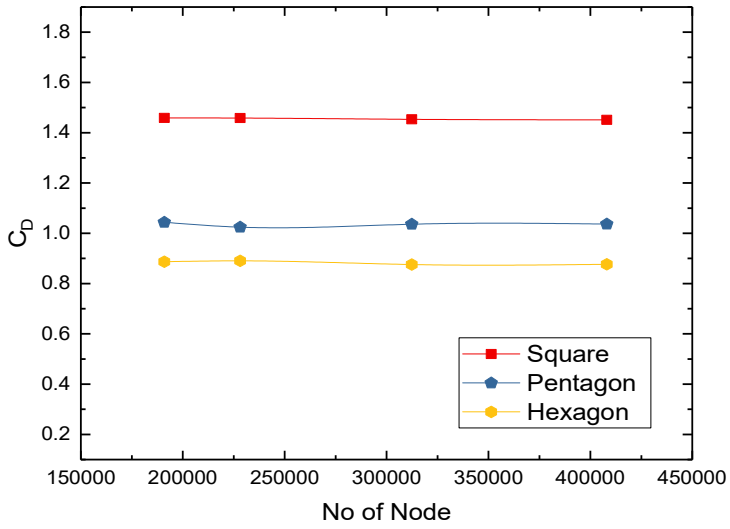

Figure 4. 4: Grid independency test

Y+ is another parameter which is verified for the simulation as the standard K-epsilon model requires a wall y+ value between approximately 300 and 100. Y+ used to describe how coarse or fine a mesh is for a particular flow pattern. A faster flow near the wall will produce higher values of y+, so the grid size near the wall must be reduced.

CHAPTER-5

RESULTS AND DISCUSSION

5.1 General

In this chapter the results of the experimental and numerical investigation regarding the surface static pressure coefficients, drag and lift coefficients have been discussed. First of all, the static pressure coefficients on the surface of square, pentagonal and hexagonal cylinders at various angles of attack are taken into consideration. Then the distributions of the static pressure coefficients on the surface of the cylinders in group from numerical study is compared. The calculated drag and lift coefficients for the group of cylinders are also presented in the same way.

5.2 Distribution of Pressure, Drag and Lift Coefficients

In this section the distributions of the pressure coefficients, drag and lift coefficients have been taken into consideration for discussion for square, pentagonal and hexagonal cylinders at different angles of attack. Pressure coefficients have been calculated from the measured values of the surface static pressures. Then the drag and lift coefficients have been obtained from the pressure coefficients by the numerical integration method.

Before going to discuss the results of the experimental investigation, it will be relevant here to present the typical flow pattern over a single square cylinder at zero, small and moderate angles of attack as shown in Figure 5.1 [52]. Although the square, hexagonal and pentagonal cylinder will give a bit different flow pattern, formation of the vortex pair will be similar. Therefore, the typical flow over the single square cylinder has been discussed. As the angle of attack increases, the path of the shear layers is altered from their point of origin at the front corners of the square cylinder to the vortex formation region as shown in Figure 5.1, In the absence of turbulence in the incident flow, the shear layers which originate at the front corners of the square cylinder curve outward and form the familiar vortex street in the wake close behind the body. The pressure developed on the back surface depends on the distance of the vortices. The longer is the distance of the vortices from the body, higher is the back pressure and vice versa. For the above reasons, pressure increases at the rear surface of the model cylinder at smaller angle of attack, while in the higher range of angle of attack, pressure decreases.

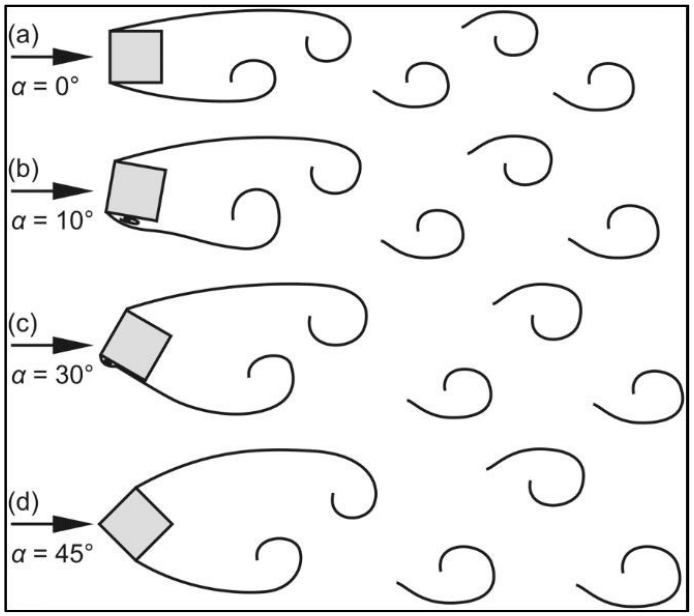

Figure 5. 1: Typical Vortex Pattern in the Downstream of Square Cylinder [52]

The pressure coefficients at different tapping points for Square, Hexagonal and Pentagonal cylinders are discussed here. The cross-section of the cylinders with five tapping on each surface of the cylinder at different AOA, the distributions of pressure coefficients for all angles of attack have been shown for relative comparison in Figures 5.2 to 5.4.

Comparative data of pressure coefficient at different faces of square shape from experimental analysis and simulation at different angles of attack has been shown in Figure 5.5. Pressure coefficient for each tapping point has been determined from the measured surface static pressure. Similarly, in Figures 5.6 and 5.7, the distributions of static pressure coefficients at different angles of attack for Pentagonal and Hexagonal shapes have been presented. In Figure 5.8, pressure contour is shown for various AOA.

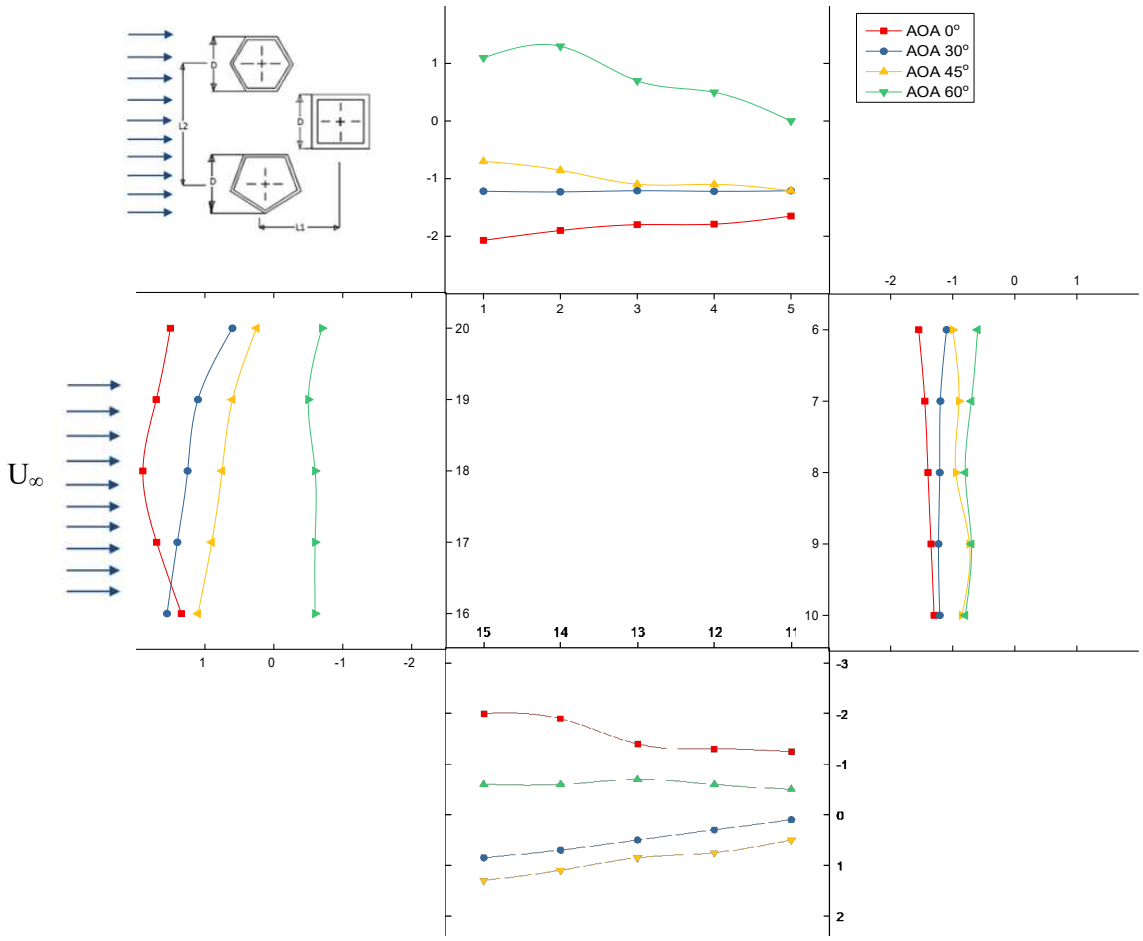

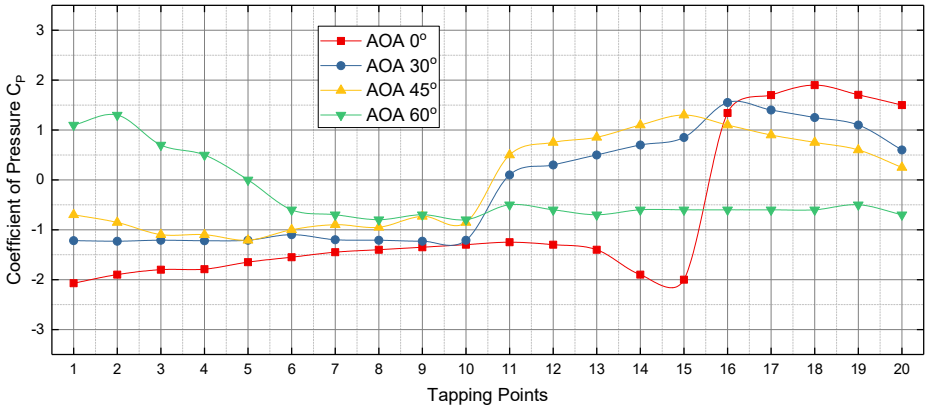

Figure 5. 2: Distribution of Pressure Coefficient on Four Faces of Square Cylinder at Different Angle of Attack

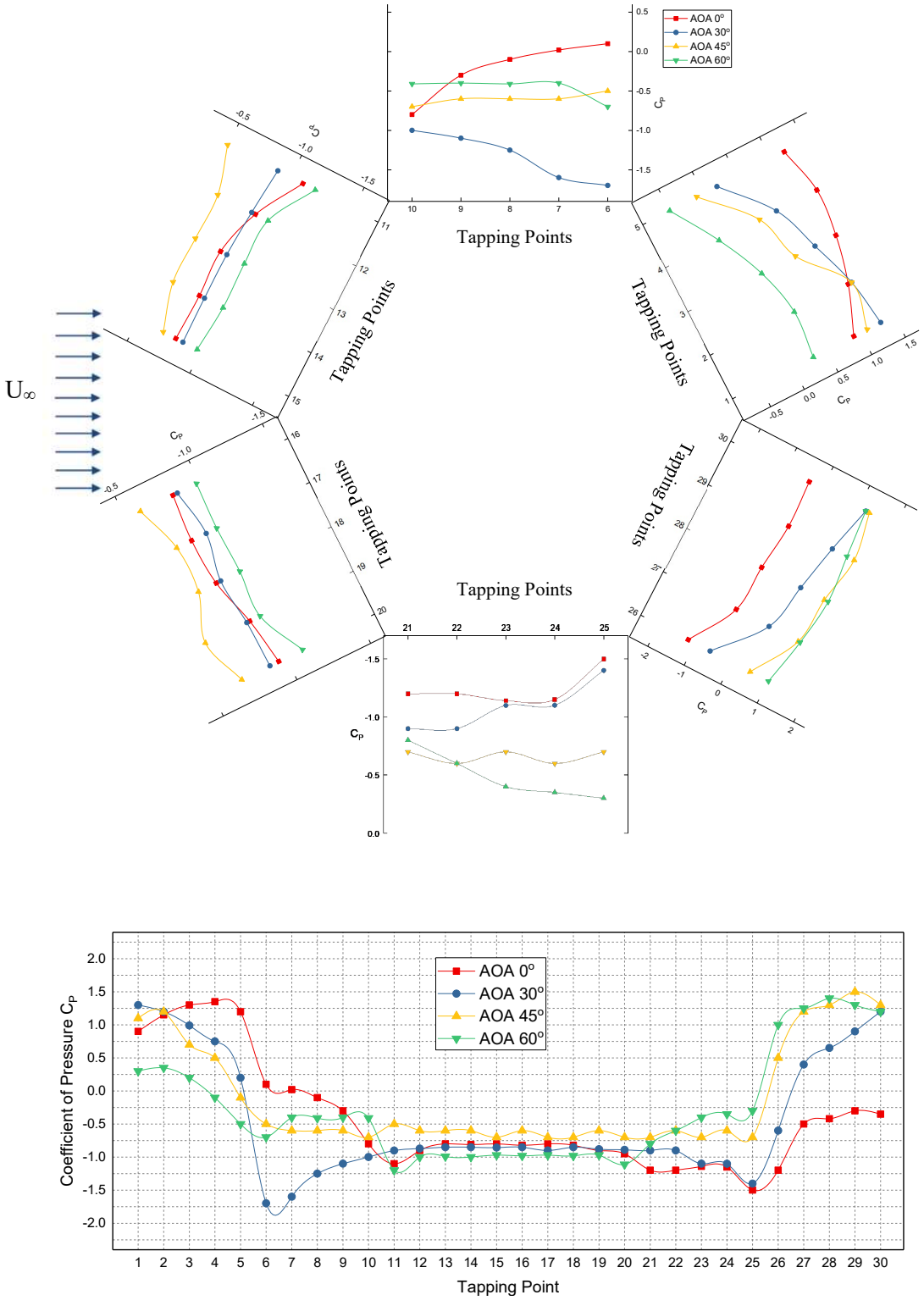

Figure 5. 3: Distribution of Pressure Coefficient on Hexagonal Cylinder at Different Angle of Attack

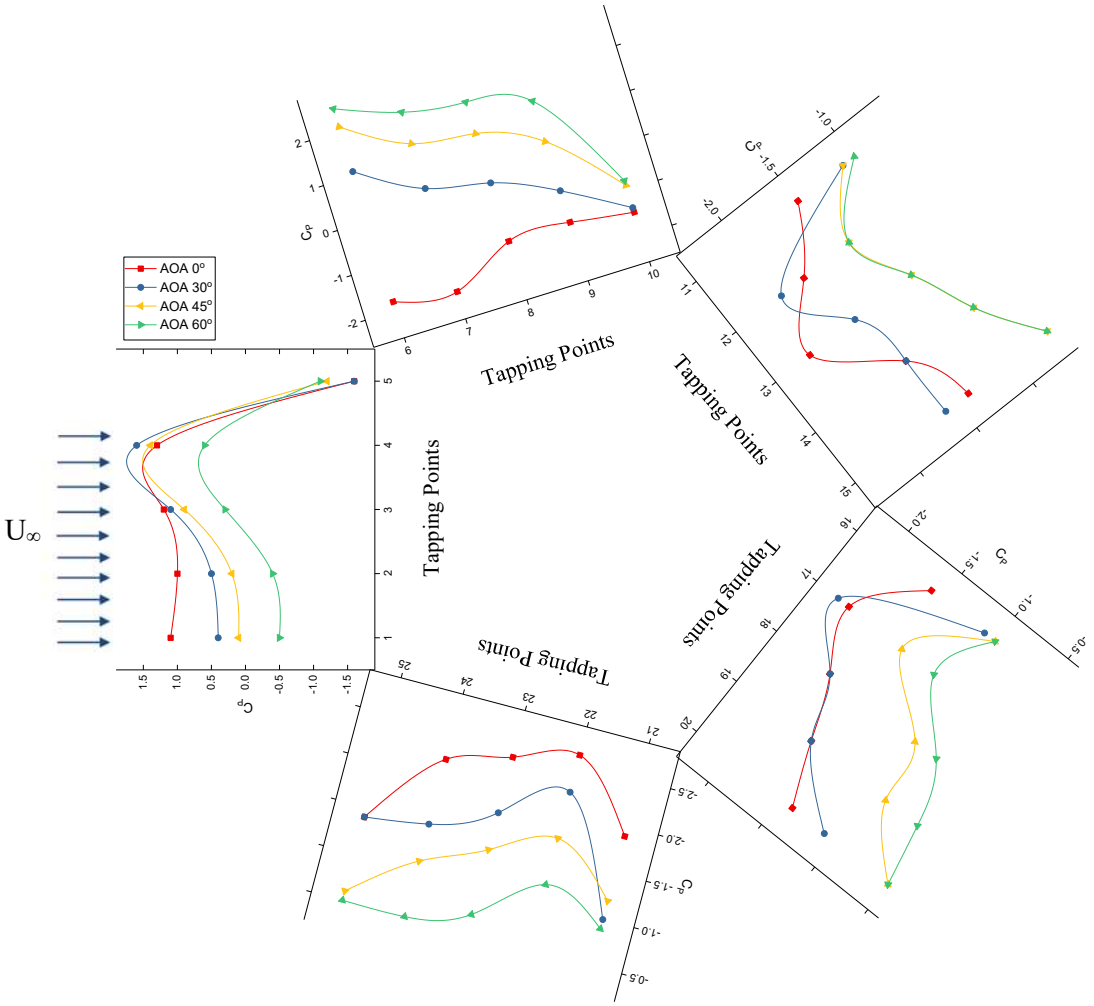

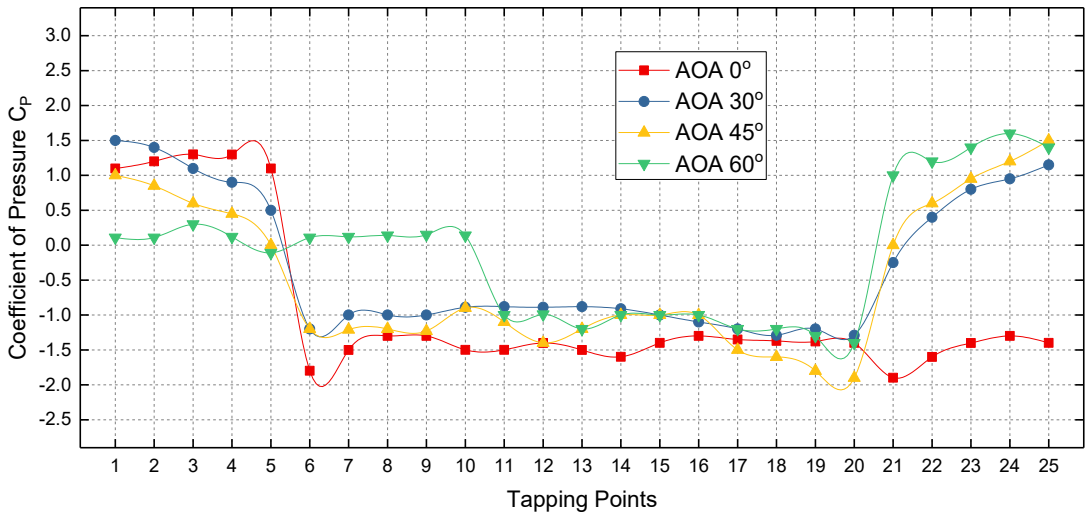

Figure 5. 4: Distribution of Pressure Coefficients at Different Angles of Attack on Pentagonal Cylinder

Square cylinder is placed in the downstream side. In different angles of attack, the variation of coefficient of pressure is shown in Figure 5.5 (a-d). Here, the comparison of experimental and simulation result can be visualized. Tapping points 16 to 20 is the wind facing side, as shown in the sketch earlier. At an angle of attack of 0˚, the wind facing side has developed maximum static pressure, which indicates the stagnation. As the AOA is increased, the position of higher static pressure has changed. Apart from that, if experimental and numerical investigations are compared, the difference in magnitude would be noticed. It is due to the smoothness of the surface in case of simulation which helps the air to glide over the surfaces. Similarity of pattern of the graph of coefficient of pressure in both cases confirms the agreement.

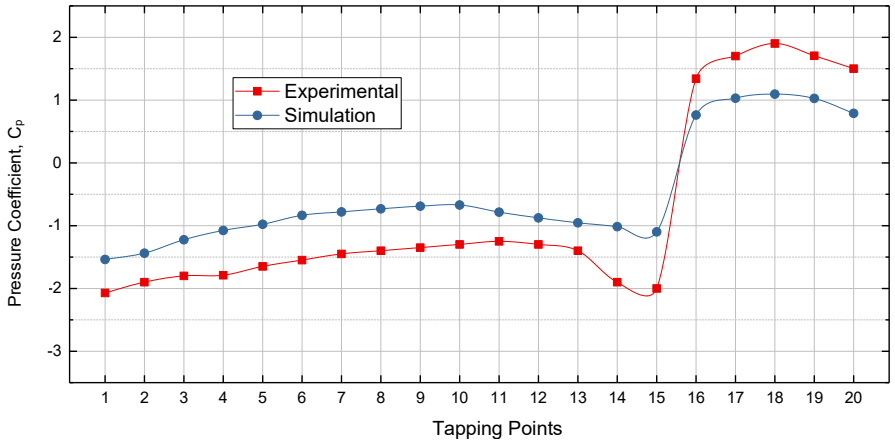

(a) Angle of Attack 0^0

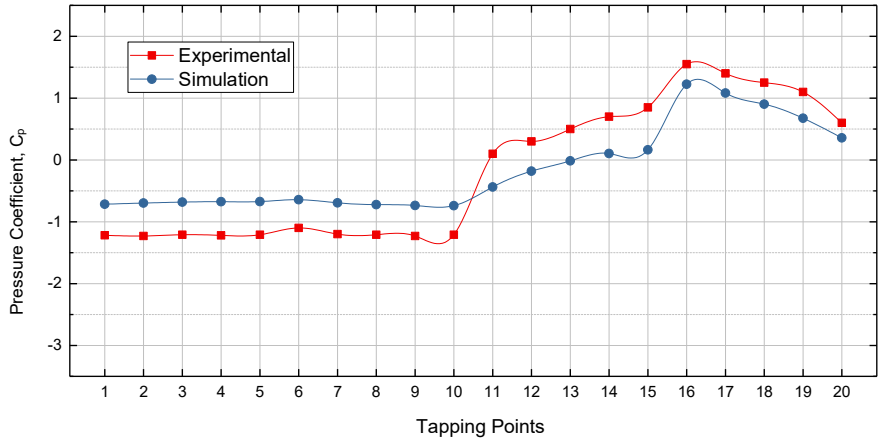

(b) Angle of Attack 30^0

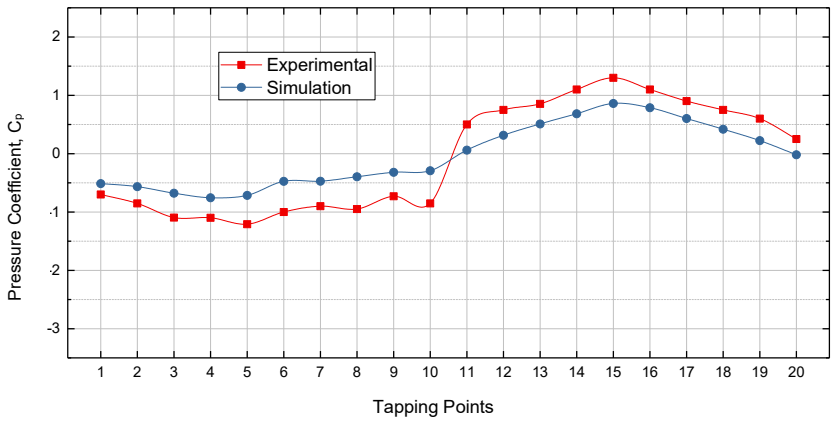

(c) Angle of Attack 45^0

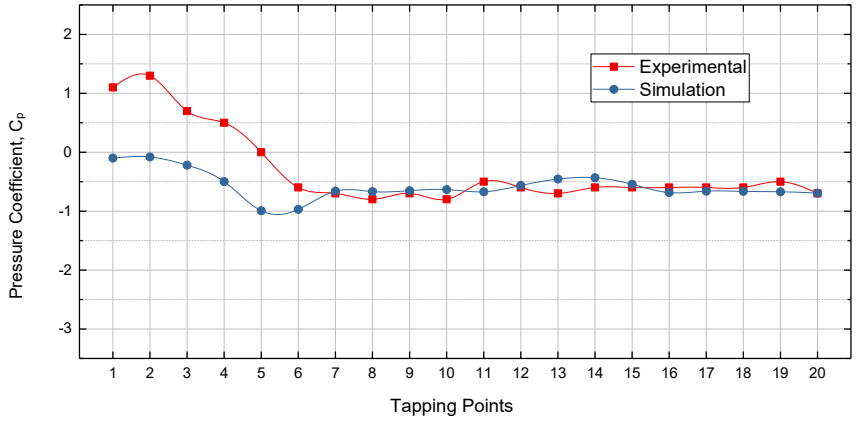

(d) Angle of Attack 60^0

Figure 5. 5: Distribution of Pressure Coefficient on Square Cylinder at (a) Angle of Attack 0^0, (b) Angle of Attack 30^0, (c) Angle of Attack 45^0, (d) Angle of Attack 60^0

Hexagonal cylinder is placed in the upstream side along with pentagonal cylinder in a parallel position. In different angles of attack, the variation of coefficient of pressure is shown in Figure 5.6 (a-d). From the comparison of experimental and simulation results, expected pattern of distribution of pressure coefficient is observed. Tapping points 1 to 5 in the wind facing side is shown in the sketch earlier. At an angle of attack of 0˚, the wind facing side has developed maximum static pressure, which indicates the stagnation. And it has decreased in next three faces of the cylinder. In the opposite side of the wind loading, the coefficient of pressure has increased in a fragment. This is because of the back flow. As the AOA increases, in 30˚ and 45˚, the distribution of coefficient of pressure is symmetric in front and back faces

but, in the opposite side of the wind loading, the coefficient of pressure increases quite significantly. In the AOA of 60˚, similar pattern like AOA of 0˚ is observed with reduced magnitude of coefficient of pressure. Apart from that, if experimental and numerical investigations are compared, similar to square cylinder, due to the smoothness of the surface in case of simulation a difference in magnitude is observed. From the similarity of pattern of the graph of coefficient of pressure in it is evident that numerical results agree well with the experimental results.

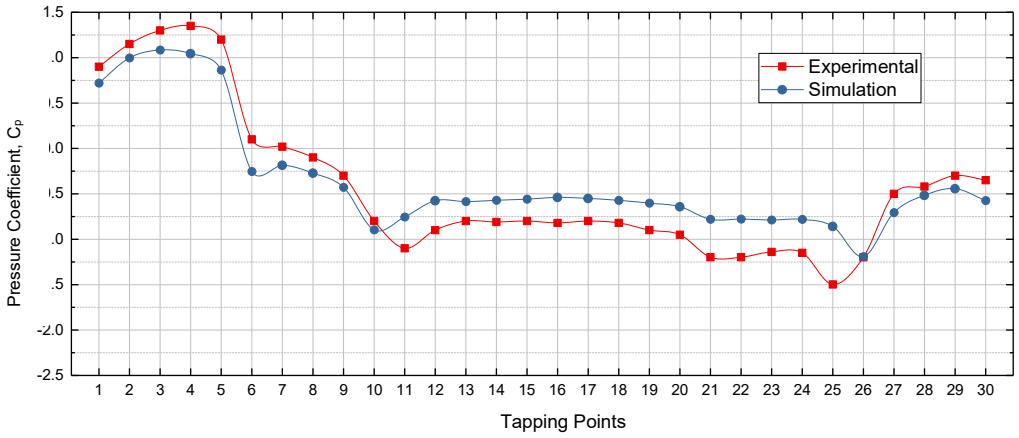

(a) Angle of Attack 0^0

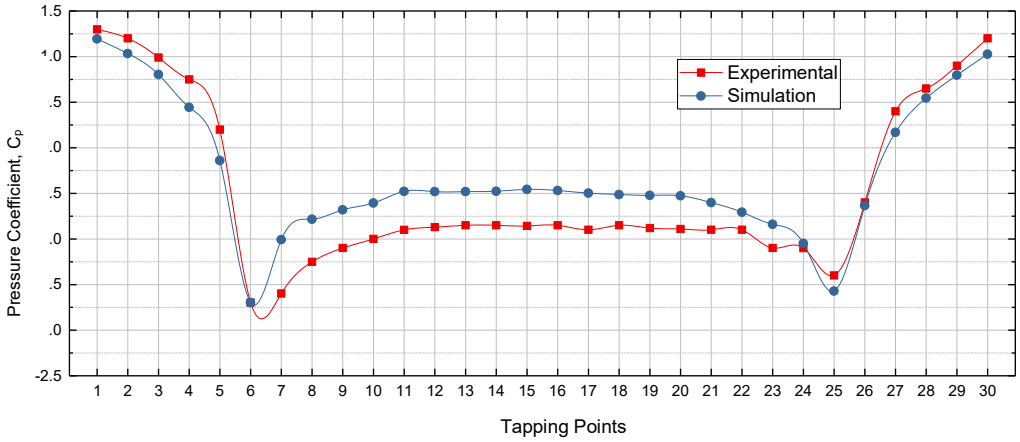

(b) Angle of Attack 30^0

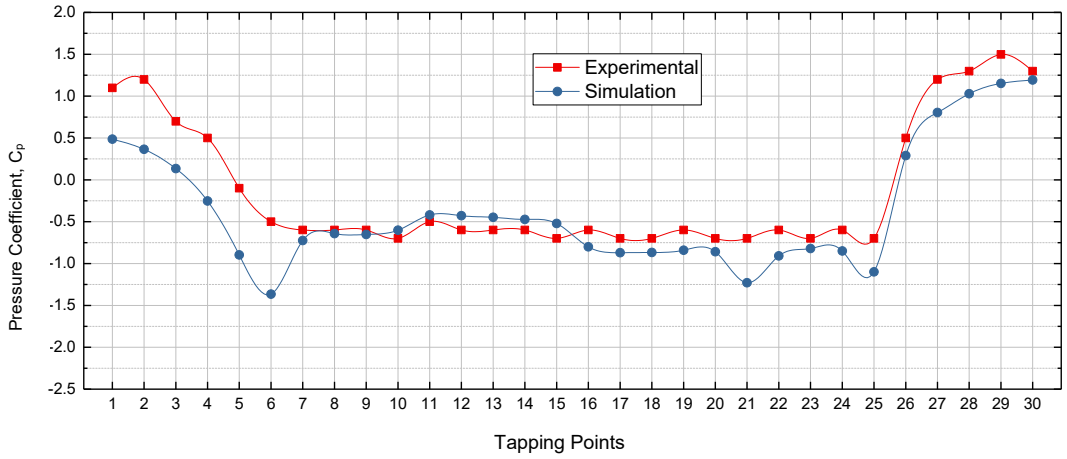

(c) Angle of Attack 45^0

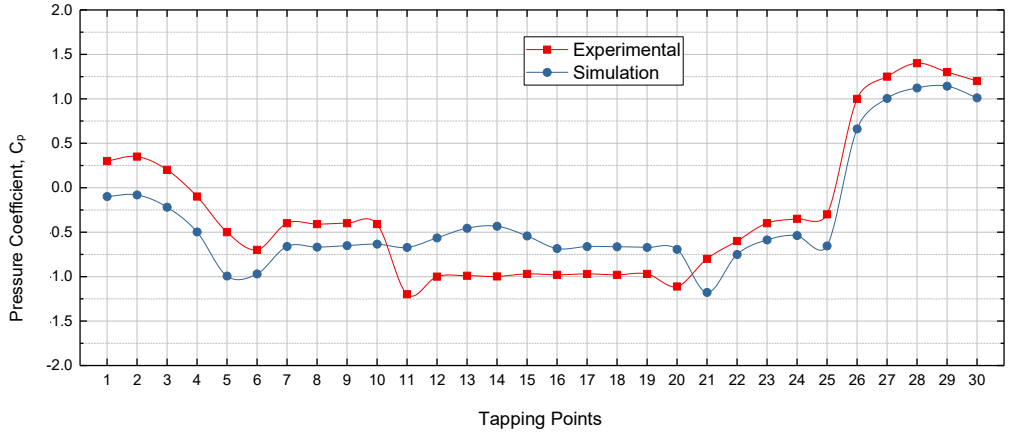

(d) Angle of Attack 60^0

Figure 5. 6: Distribution of Pressure Coefficient on Hexagonal Cylinder at (a) Angle of Attack 0^0, (b) Angle of Attack 30^0, (c) Angle of Attack 45^0, (d) Angle of Attack 60^0

Pentagonal cylinder is placed in the upstream side along with hexagonal cylinder in a parallel position. In different angles of attack, the variation of coefficient of pressure is shown in Figure 5.7 (a) to Figure 5.7 (d). From the comparison of experimental and simulation results, usual pattern can be observed. Tapping points 1 to 5 is the wind facing side, as shown in the sketch earlier. At an angle of attack of 0˚, the wind facing side has developed maximum static pressure, which indicates the stagnation. And it is decreased in next two faces of the cylinder. In the opposite side of the wind loading, the coefficient of pressure is increased in smaller amount. This is because of the back flow. As the AOA increases, in 30˚ and 45˚, the distribution of coefficient of pressure is symmetric in front and back faces. In the AOA of

60˚, location of the stagnation is changed. Apart from that, if experimental and numerical investigations are compared, similar to square cylinder, due to the smoothness of the surface in case of simulation a difference is magnitude is observed. Similarity of pattern of the graph of coefficient of pressure in both cases confirms the cogency.

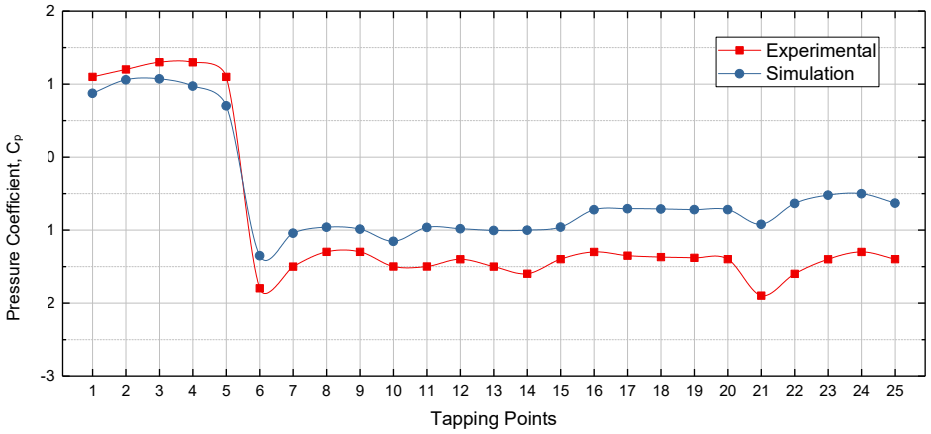

(a) Angle of Attack 0^0

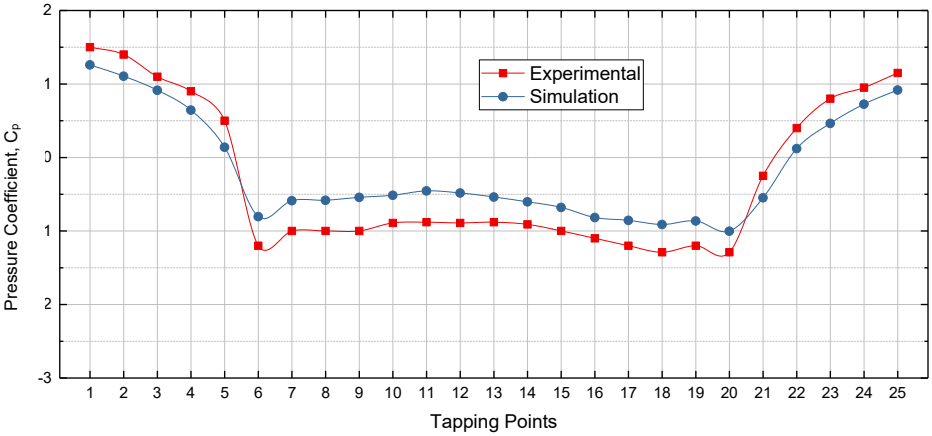

(b) Angle of Attack 30^0

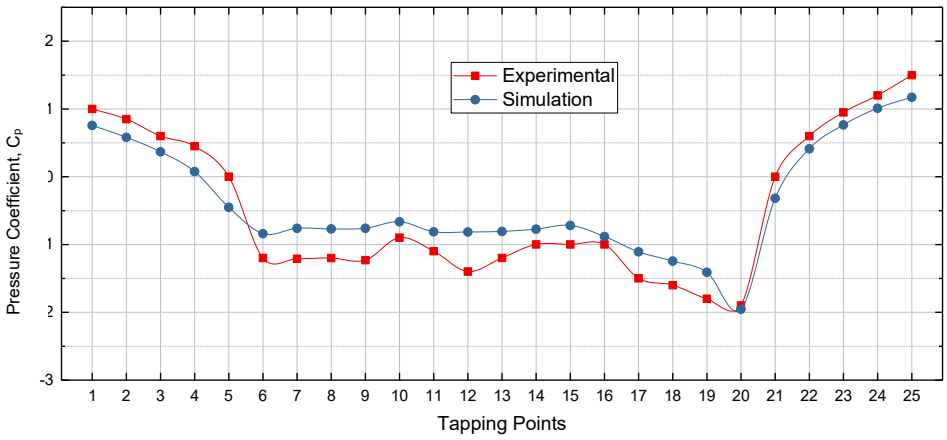

(c) Angle of Attack 45^0

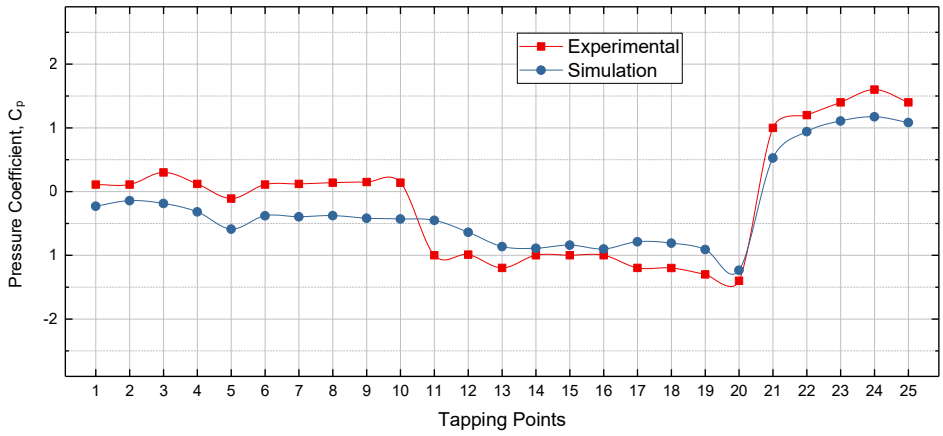

(d) Angle of Attack 60^0

Figure 5.7: Distribution of Pressure Coefficient on Pentagonal Cylinder at (a) Angle of Attack 0^0, (b) Angle of Attack 30^0, (c) Angle of Attack 45^0, (d) Angle of Attack 60^0

In next Figures of 5.8 (a) to 5.8 (d), 5.9 (a) to 5.9 (d) and 5.10 (a) to 5.10 (d), pressure contour, velocity streamline and velocity contour are represented respectively. The pressure contour provides a visual understanding of previous explanation of distribution of the coefficient of pressure. From the Figure of 5.9 (a) to 5.9 (d), it can be noticed that flow separation is created in the wake region at angles of attack of 30˚ and 45˚. In case of 0˚ and 60˚, back flow is present. Also, the velocity is higher at adjacent surface of the wind facing side as the wind flows through the contact surface. On the other hand, if magnitude of coefficient of pressure is concerned at wind facing side, then square shaped cylinder is resulting in less in numerical because of the arrangement.

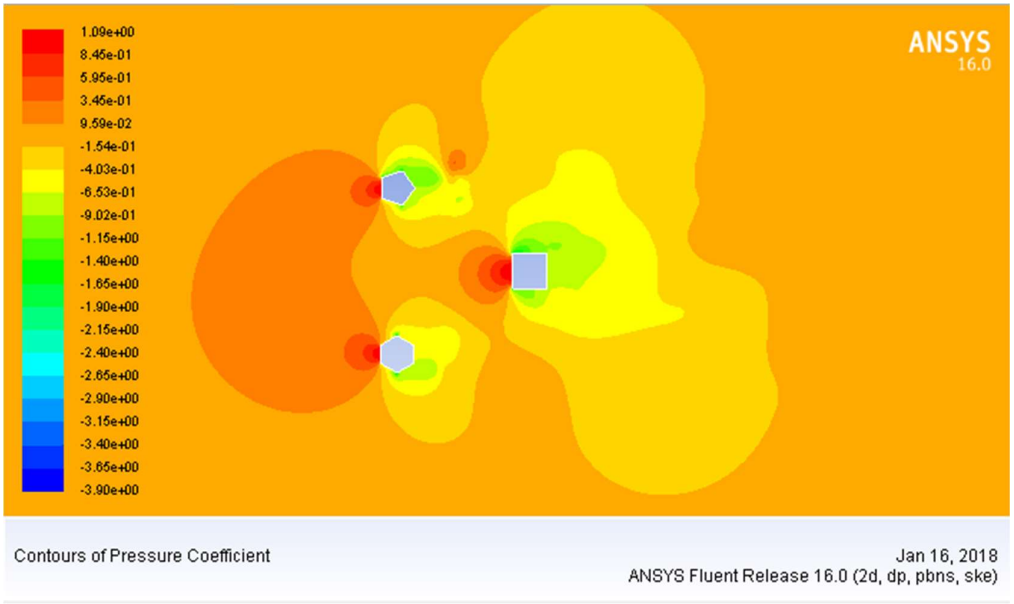

(a) Angle of Attack 0^0

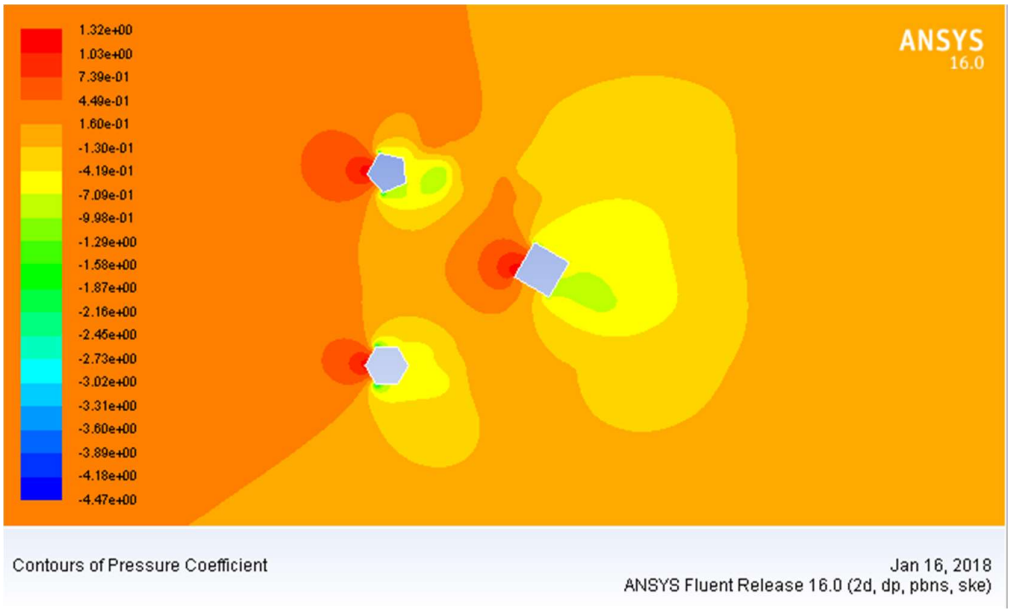

(b) Angle of Attack 30^0

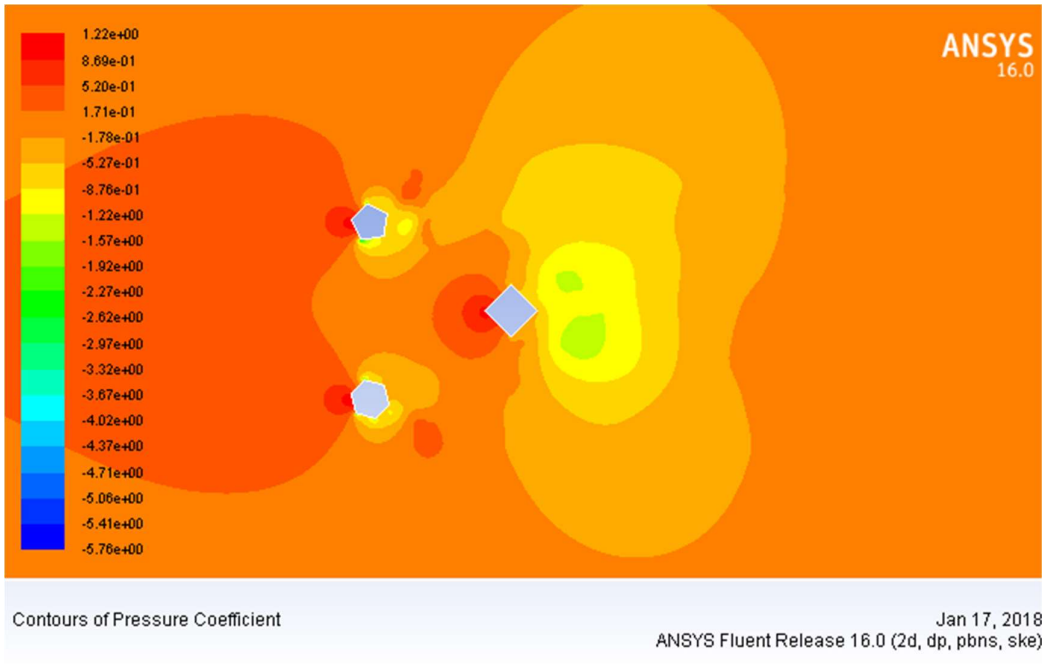

(c) Angle of Attack 45^0

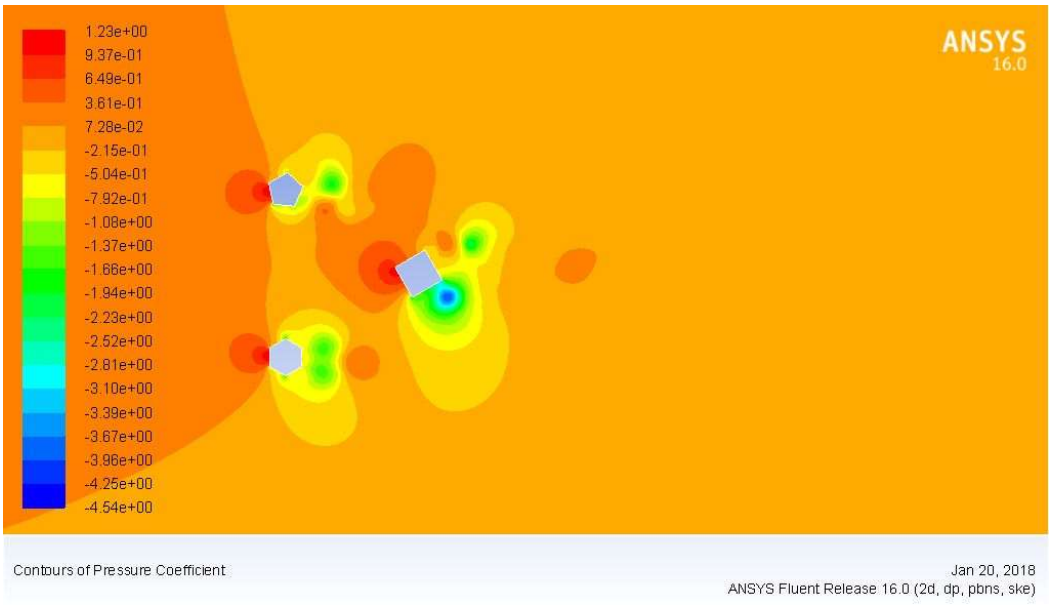

(d) Angle of Attack 60^0

Figure 5.8: Contours of Pressure Coefficient at (a) Angle of Attack 0^0, (b) Angle of Attack 30^0, (c) Angle of Attack 45^0, (d) Angle of Attack 60^0

5.3 Velocity Streamline and Velocity Contour:

Velocity streamline and velocity contours provide an excellent impression of the flow to understand the change in velocity and nature of flow of air around the group of cylinders. From figure 5.9 (a), it is observed that at 0˚, velocity is reduced at the front face and air glides towards vertical sides and red color indicates that velocity increment towards the flow direction.

Maximum drag is observed at 30˚ angle of attack for all three cylinders and interference of flow including flow separation and backflow are observed at 60˚ angle of attack for square and at 30˚ angle of attack for Pentagonal and Hexagonal when having their corners towards upstream i.e. each section has two surfaces at a steep angle with the flow direction.

In figure 5.9 and 5.10, the light bluish green color in the downstream areas show how the group of cylinders influence the airflow around and behind them. The red colors indicate the venturi effect between the cylinders and dark blue areas show the eddies behind the cylinders.

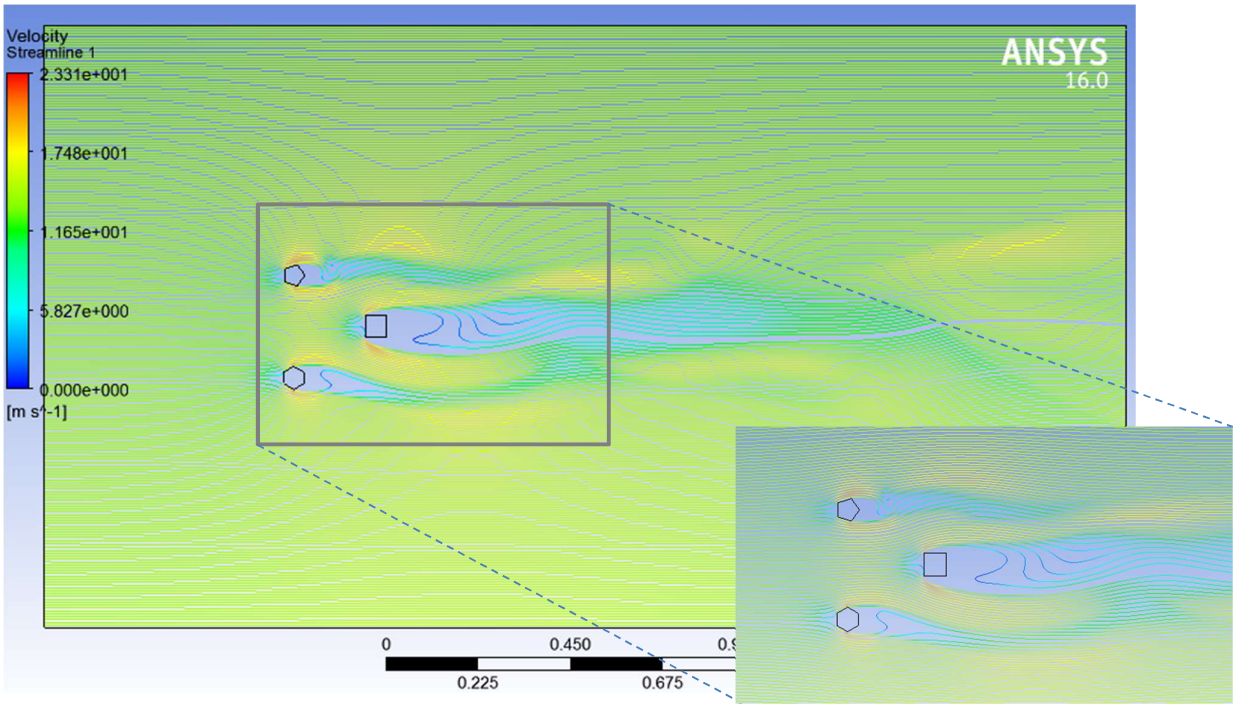

(a) Angle of Attack 0^0

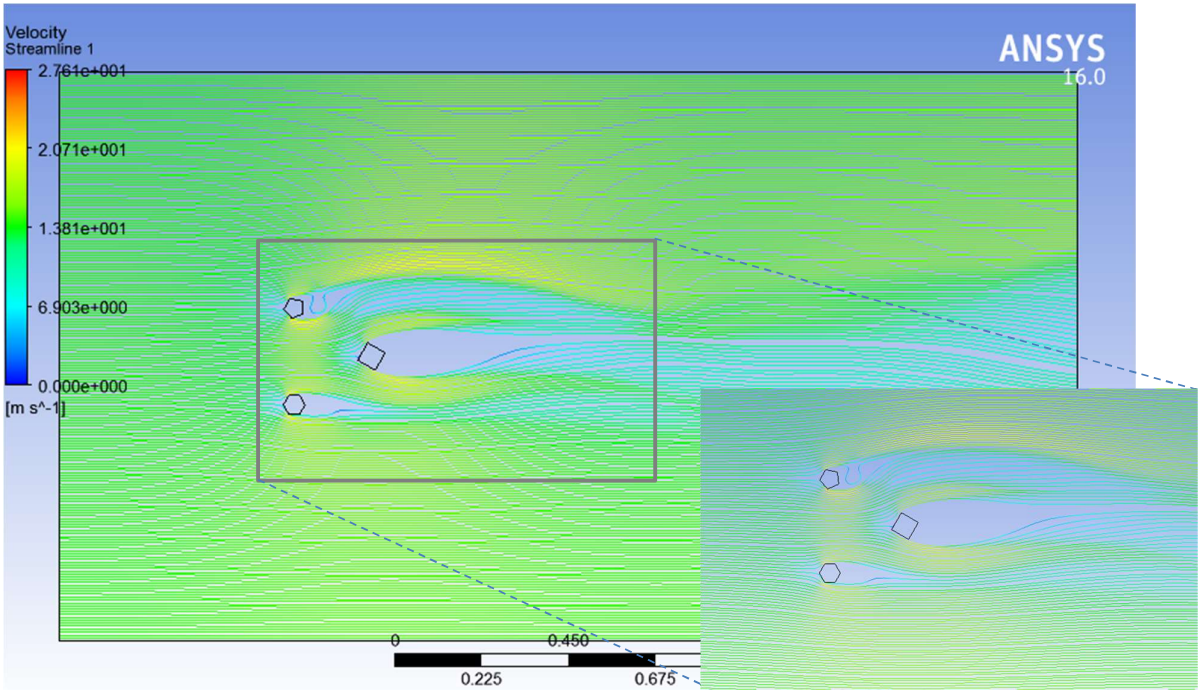

(b) Angle of Attack 30^0

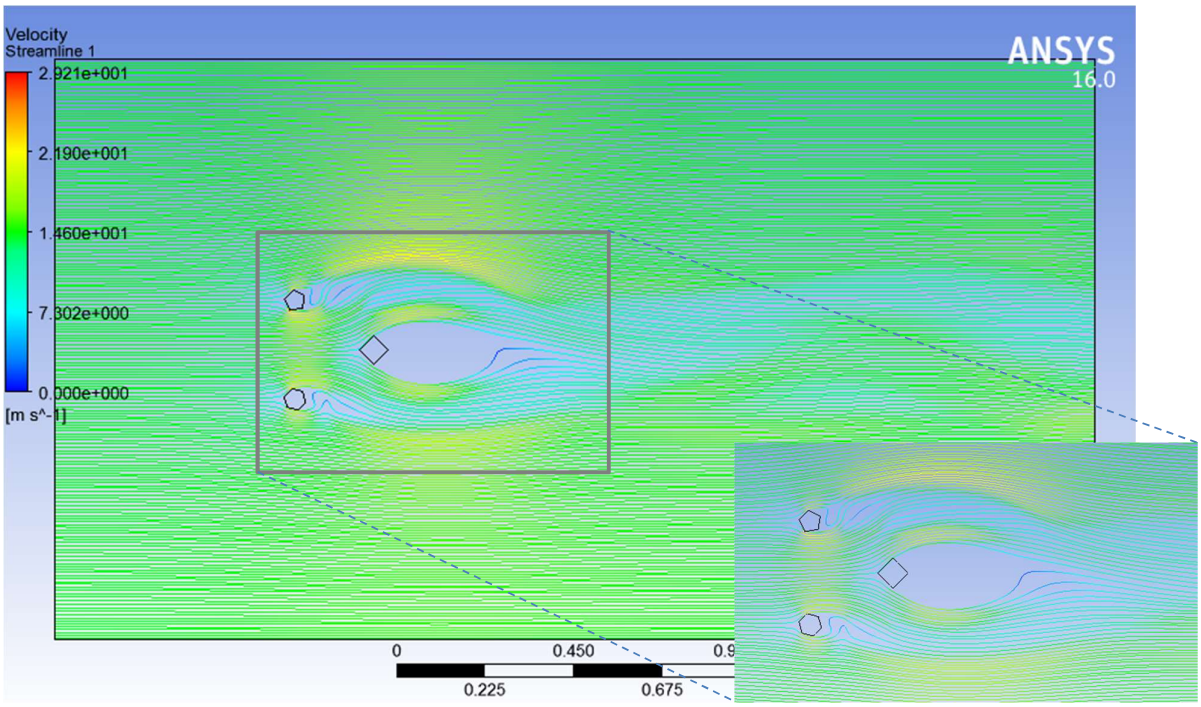

(c) Angle of Attack 45^0

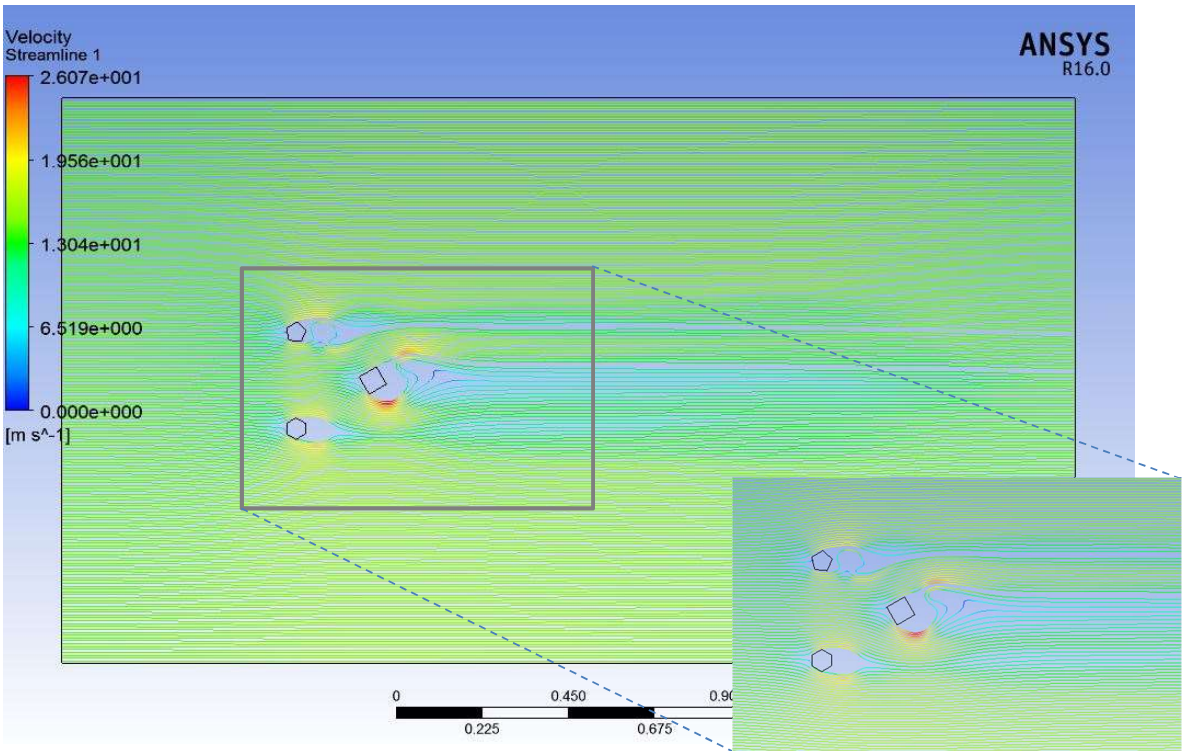

(d) Angle of Attack 60^0

Figure 5.9: Velocity Streamline at (a) Angle of Attack 0^0, (b) Angle of Attack 30^0, (c) Angle of Attack 45^0, (d) Angle of Attack 60^0

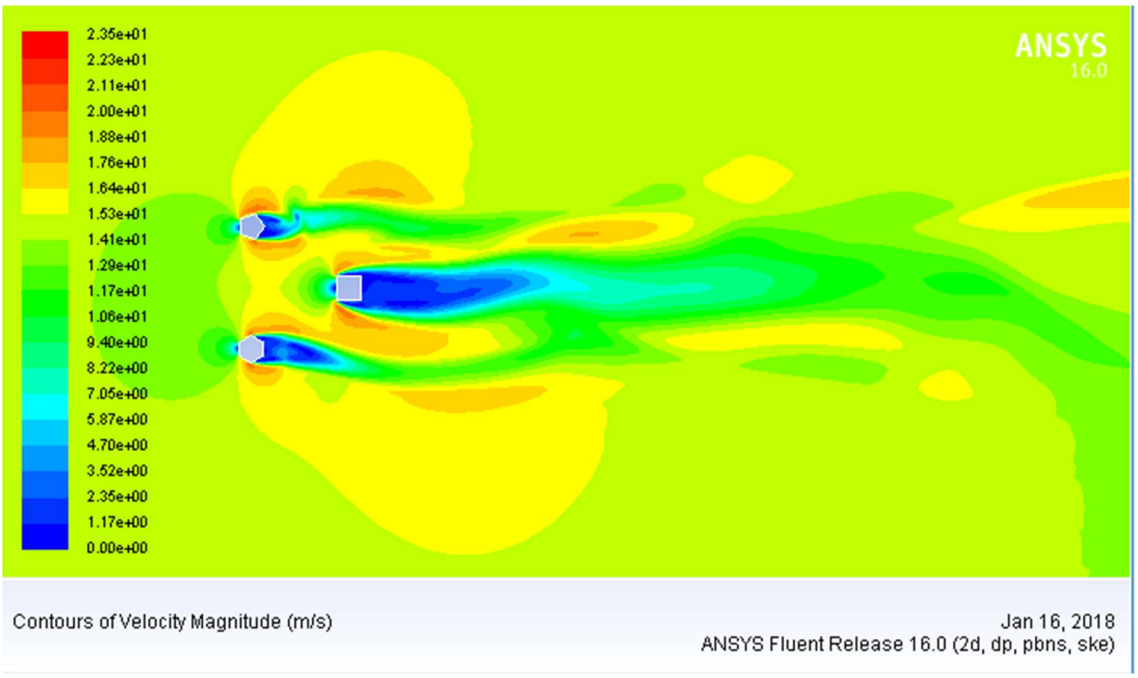

(a) Angle of Attack 0^0

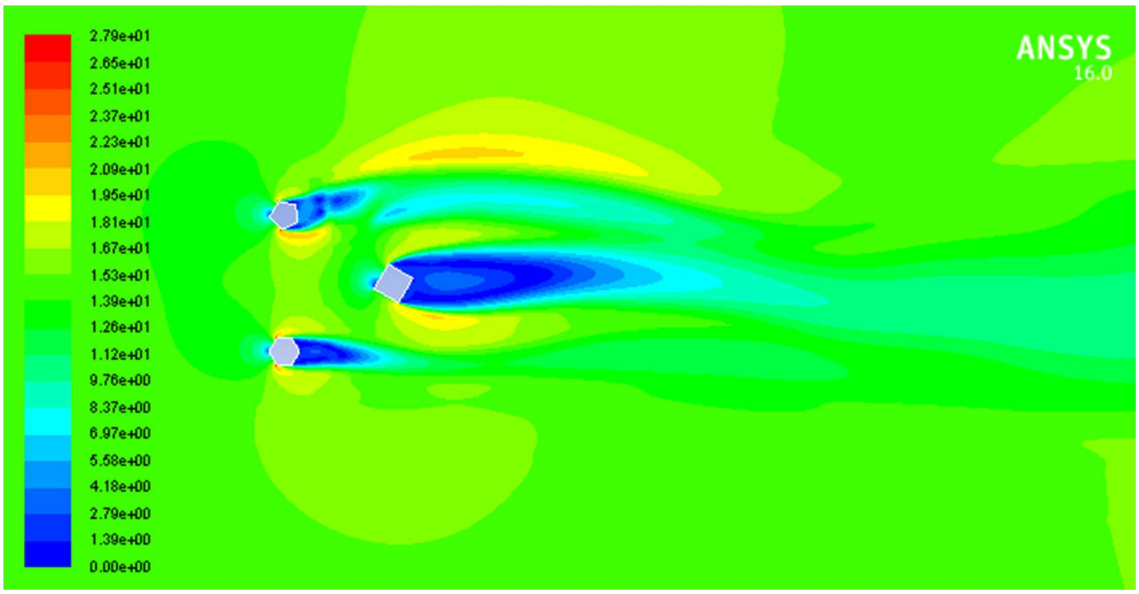

(b) Angle of Attack 30^0

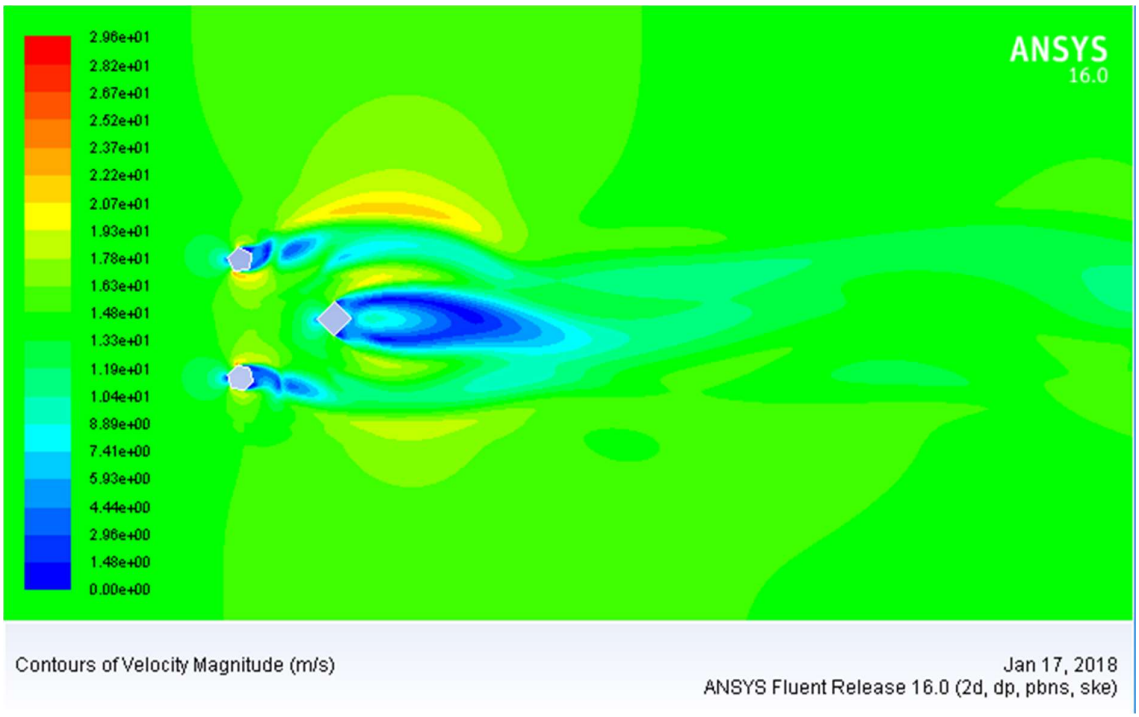

(c) Angle of Attack 45^0

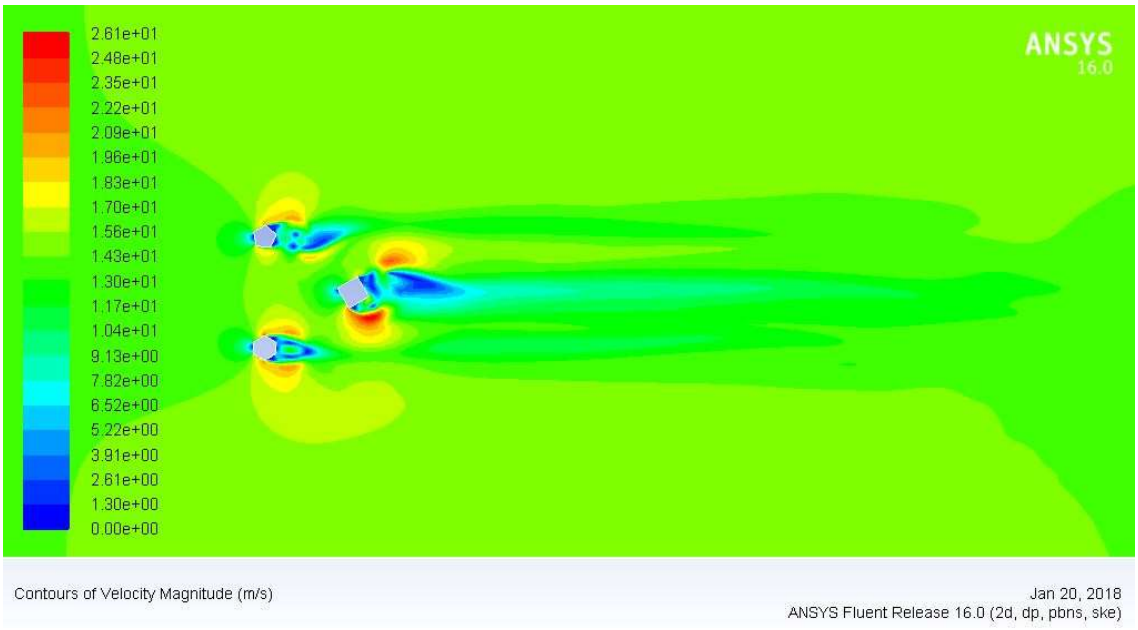

(d) Angle of Attack 60^0

Figure 5.10: Contours of Velocity Magnitude at (a) Angle of Attack 0^0, (b) Angle of Attack 30^0, (c) Angle of Attack 45^0, (d) Angle of Attack 60^0

5.4 Variation of Drag and Lift Coefficient for Different Shapes

In Figures 5.11 and 5.12, the variation of drag and lift at different AOA for different shapes are presented. Maximum drag and minimum lift is attained at angle of attack of 30˚ for square shape structure. Here it should be noted that this drag is a prediction of the force acting on the structure itself. From these representations, a suitable arrangement can be recommended for these specific shapes.

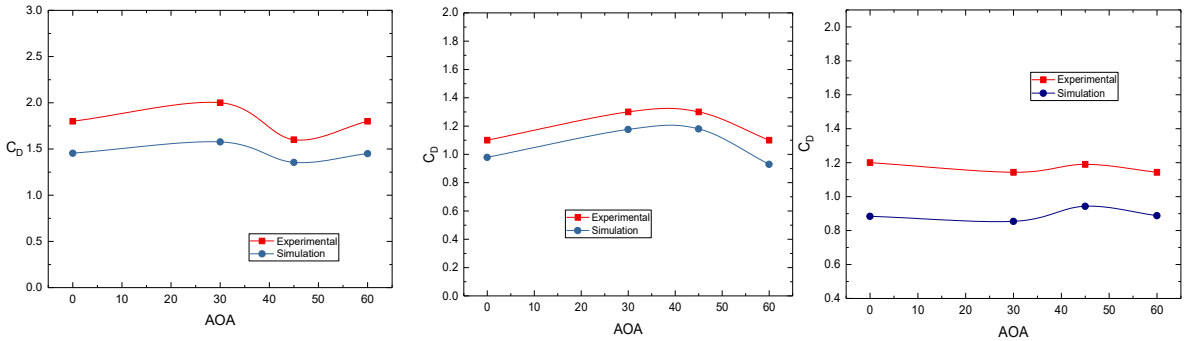

Figure 5.11: Variation of Coefficient of Drag at different angles of attack for (a) Square structure, (b) Pentagonal structure, (c) Hexagonal structure

Furthermore, in the calculation of coefficient of drag the experimental values exceed the values of simulation and vice versa in the calculation of coefficient of lift because of the availability of smoother surface in case of simulation. In actual case, the discontinuation on the surface and roughness present will drastically increase the drag force acting on the structure. Hence, a correction factor may be optimized and used in calculation.

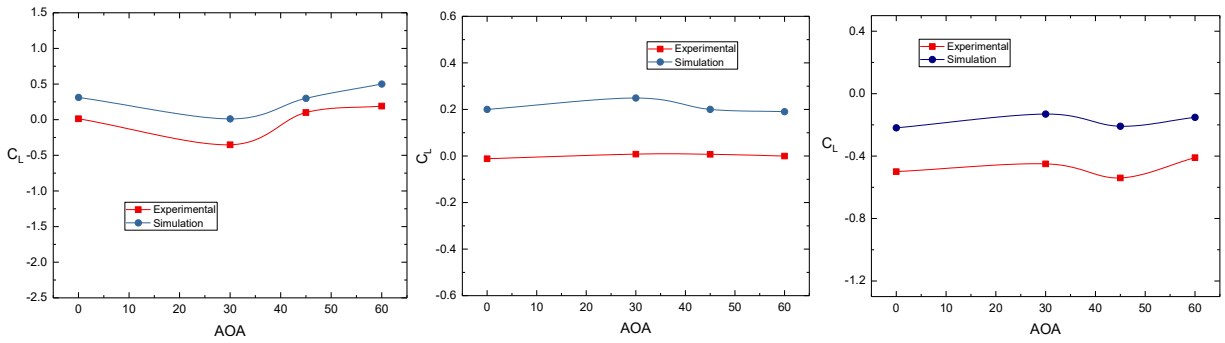

Figure 5.12: Variation of Coefficient of Lift at different angles of attack for (a) Square structure, (b) Pentagonal structure, (c) Hexagonal structure

From a different point of view, significance of effect of Reynold's number is also dependent on shape of the structure. From figure 5.13, it is visible that, at 30˚ of angle of attack, value of coefficient of drag increases for square shape at a higher rate than other two structures, with increasing Reynolds number (i.e. with increasing free stream velocity). Also, magnitude of C_D is higher for square shape than other two.

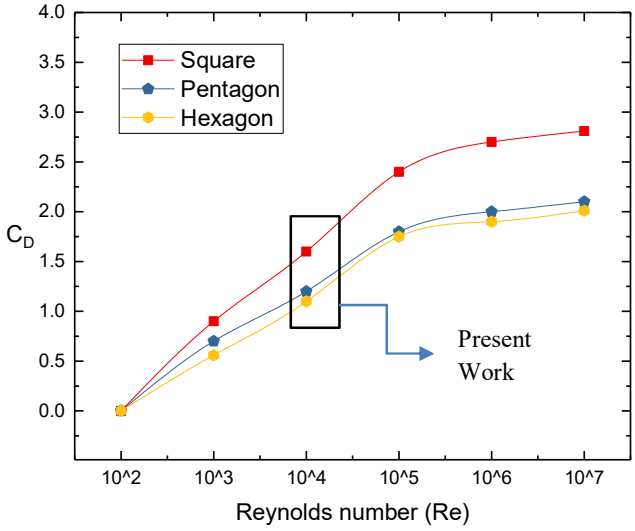

Figure 5. 13: Variation of Coefficient of Drag with Reynolds Number at 30˚ AOA for different structures

To further concentrate on the variation of drag and lift forces due to the structure and arrangement, comparison with the result of a similar arrangement is illustrated here which was done by Rizia [52]; where a group of pentagonal, hexagonal and octagonal shaped structures is subject to wind flow of same Reynold's number. Here octagonal structure is kept at the downstream side. As the octagonal structure is close to circular shape, hence, coefficient of drag is of less value than that of a square shape. Also, it is observed that in case of upstream cylinders as well, the magnitude of C_D is less when an octagonal structure is used at the downstream side. Hence, presence of downstream cylinder has an impact on the magnitude of C_D on the surfaces of upstream cylinder.

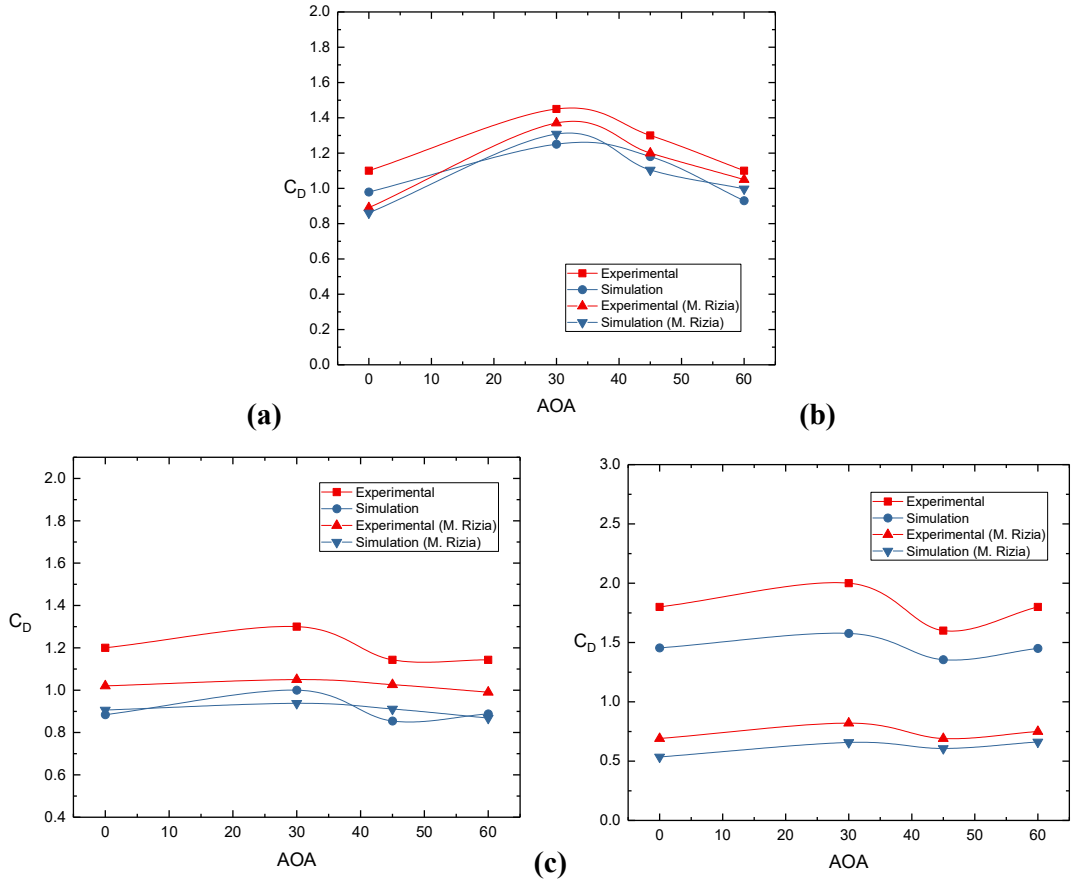

Figure 5.14: Variation of Coefficient of Drag at different angles of attack for (a) Pentagonal structure, (b) Hexagonal structure, (c) Downstream structure

In case of downstream structure, because of change in shape, that is Octagonal structure is closer to circular shape, has encountered almost one-third of the drag force which has been experienced by the square structure in the present work, as can be observed in figure 5.14. This validates the existence of effect of shape and arrangement in case of wind loading. In

the Comparison of C_L values, from figure 5.15, it is found to be very small with little variation in average magnitude and close to zero for all cylinders.

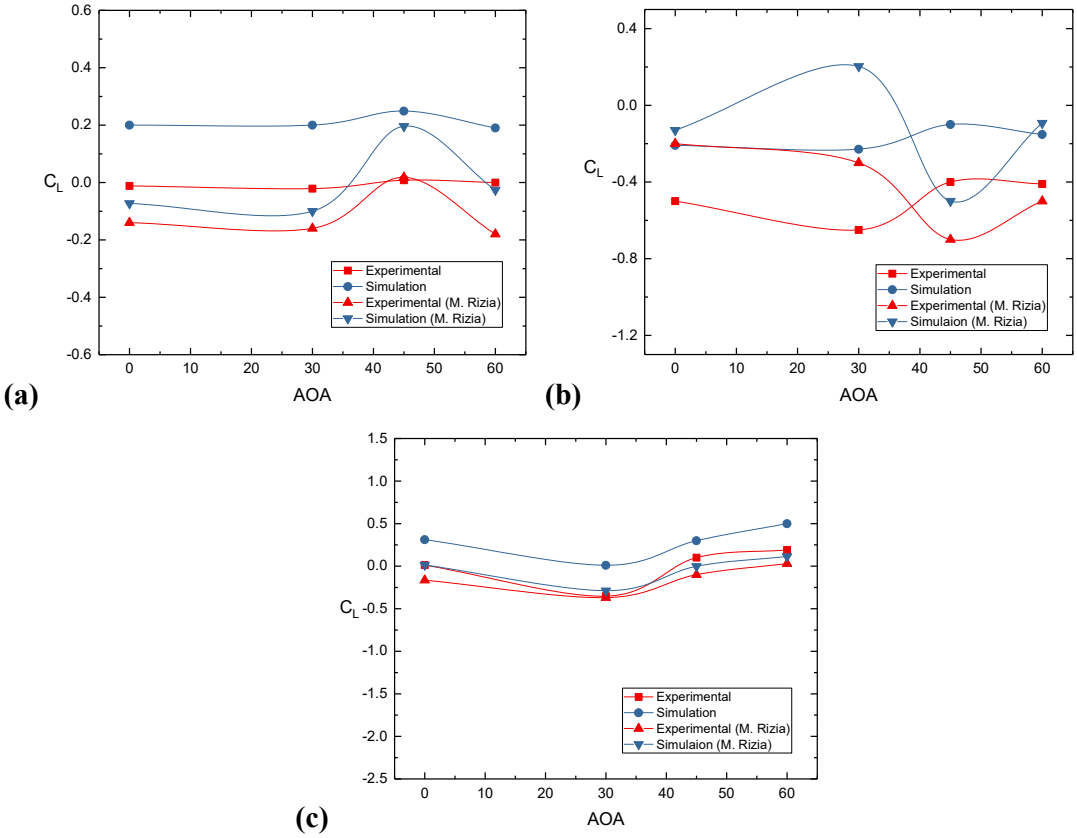

Figure 5.15: Variation of Coefficient of Lift at different angles of attack for (a) Pentagonal structure, (b) Hexagonal structure, (c) Downstream structure

5.5 Error in Measurements

During measurement of the surface static pressures on the cylinders for several days, the room temperature is assumed to be constant. As such the density of the air is taken as constant in the calculation. In reality, there is minor variation of the temperature during taking all the readings, which has been neglected in the calculation. The fluctuation of the manometer reading was observed especially on the suction side of the cylinders. But that fluctuation was not significant. While taking the reading, always the mean value of the manometer was recorded. Since fluctuation was insignificant the error in the measured values was negligible.

CHAPTER-6

CONCLUSIONS AND RECOMMENDATIONS

6.1 Conclusions

The following conclusions are drawn in regard to the effect of shapes and arrangement of solid cylinders in wind loading.

a) Overall, the drag coefficient for a square cylinder at all angle of attack is more in contrast to that of for a hexagonal and pentagonal cylinder at the same angle of attack.

b) There is significant rise in the drag coefficient values for the square cylinder (downstream) in comparison to that of the other two cylinders (upstream) whereas in previous works, it was seen that when two cylinders are placed at downstream and one at upstream; there is drop in the drag coefficient at downstream. This is due to the difference in arrangement and structure of downstream cylinder. This confirms the impact of the shape of downstream cylinder on the magnitude of C_D of upstream cylinder.

c) The variation of the lift coefficient on cylinders is not significant and they are nearly zero, but in case of 30˚ angle of attack in square cylinder, substantial drop to lowest value is observed.

d) Maximum drag is observed at 30˚ angle of attack for all three cylinders and interference of flow including flow separation and backflow are observed at 60˚ angle of attack for square and at 30˚ angle of attack for Pentagonal and Hexagonal when having their corners towards upstream i.e. each section has two surfaces at a steep angle with the flow direction.

e) Simulation results agree well with the experimental results although there is variation at magnitude, therefore need of prototyping is minimized. While wind load is to be used for the design of the free-standing building and group of building having pentagonal, hexagonal and square cross-section, the outcome of the present results may be applied.

6.2 Recommendations

For further study in relation to the present work the following recommendations are provided below.

a) The flow behavior around the cylinder, wind shear, effect of Reynolds number may be taken into consideration for the study, along with variation of arrangements.
b) Model of urban canopies i.e structures of various shapes and sizes with different inter-spacing may be researched to find the wind load.
c) This work has been done on the group of different shaped structures at limited angle of attack only; increase in variation of the angle of attack may be taken into consideration.
d) Similar study can be carried out replacing the sharp corners into rounded corners to observe the effect on wind loading.

REFERENCES

[1] Baines, W. D., "Effects of Velocity Distribution on Wind Loads and Flow Patterns on Buildings", Proceedings of a Symposium on Wind Effects on Buildings and Structures", Teddington, U.K. 1963, pp. 197-225.

[2] Barriga, A. R., Crowe, C. T and Roberson, J. A., "Pressure Distribution on a Square Cylinder at a Small Angle of Attack in a Turbulent Cross Flow", Proceedings of the 4th International Conference on Wind Effects on Buildings, London, U.K. 1975, pp. 89-93.

[3] Bearman, P. W. and Truman, D. M., "An Investigation of the Flow Around Rectangular Cylinders", The Aeronautical Quarterly, Vol. 23, 1971, pp. 229-237.

[4] Biswas, N., "An Experimental Investigation of Wind load on Tall Buildings with Square Cross-section having Rounded Facet", A Master's Thesis Presented in Mechanical Engineering Department, BUET, Dhaka, January, 2008.

[5] Bostock, B. R and Mair, W. A., "Pressure Distributions and Forces on Rectangular and D-Shaped Cylinders", The Aero- Dynamical Quarterly, Vol. 23, 1972, pp. 499-511.

[6] Castro, J. P. and Fackwell, J. E., "A Note on Two- Dimensional Fence Flows with Emphasis on Wall Constant", J. Industrial. Aerodynamics, 3(1), March 1978.

[7] Islam, A. T. M. and Mandal, A. C., "Experimental Analysis of Aerodynamic Forces for Cross- flow on Single Rectangular Cylinder", Mechanical Engineering Research Bulletin, BUET, Dhaka, Vol. 13, No. 1, 1990, pp. 36-51.

[8] Farok, G. M. G., "An Experimental Investigation of Wind Effect on Rectangular Cylinders with Rounded Corners", M.Sc. thesis, BUET, 2004.

[9] Hua, C. K., "The Behavior of Lift Fluctuations on the Square Cylinders in the Wind Tunnel Test", Proceedings of the 3rd International Conference on Wind Effects on Buildings and Structures, Tokyo, Japan, 1971, pp. 911-920.

[10] Davis, R. W and Moore, E. F., "A Numerical Study of Vortex Shedding from Rectangular Cylinders". Journal of Fluid Mechanics, Vol. 116, pp. 475-506.

[11] Lee, B. E., "The Effect of Turbulence on the Surface Pressure Field of a Square Prism", Journal of Fluid Mechanics, Vol. 6 J. E. 9, Part 2, 1975, pp. 263-282.

[12] Mandal, A. C. and Farok, G. M. G., "An Experimental Investigation of Static Pressure Distributions on Square and Rectangular Cylinders with Rounded

Corners", 4th International Conference on Heat Transfer, Fluids Mechanics and Thermodynamics (HEFAT), Cairo, Egypt, September. 2005, Cairo, Egypt, Paper No: MA5.

[13] Hussain, H. S. and Islam, O., "Study of Wind Load on Buildings and Structures", Journal of the Institution of Engineers, Bangladesh, Vol. 1. No. 2-3, July - October, 1973.

[14] Hossain, M. K. M., Islam, M. Q, Mandal, A. C and Saha, S., "Wind Effect on Staggered Square Cylinders of Square and Rectangular Sections with Variable Longitudinal Spacing", Transaction of the Mechanical Engineering Division, The Institution of Engineers, Bangladesh, Vol. ME 38, Dec. 2007, pp. 52-57.

[15] Islam, A. M. T. and Mandal, A. C., "Static Pressure Distribution for Cross- flow on Single Rectangular Cylinders", Mechanical Engineering Research Bulletin, BUET, Dhaka, Vol. 14, No. 1, 1991, pp. 8-23.

[16] Islam, A. M. T. and Mandal, A. C., "Effect of Longitudinal Spacing on Static Pressure Distribution of Rectangular Cylinders", Mechanical Engineering Research Bulletin, BUET, Dhaka, Vol. 15, No. 1, 1992, pp. 22-47.

[17] Koening, K. and Roshiko, A., "An Experimental Study of Geometrical Effects on the Drag and Flow Field of Two Bluff Bodies Separated by a Gap", Journal of fluid Mechanics Vol. 156, pp. 167-204.

[18] Leutheusser, J., "Static Wind Loadings of Grouped Buildings", Proceedings of the 3rd international Conference on Wind Effects on Buildings, Tokyo, Japan, 1971, pp. 211-220.

[19] Mandal, A. C. and Farok, G. M. G., "An Experimental Investigation of Static Pressure Distributions on a Group of Square and Rectangular Cylinders with Rounded Corners", Submitted for publication in the Journal of Mechanical Engineering, The Institution of Engineers, Bangladesh.

[20] Mandal, A. C. and Islam, O., "A Study of Wind Effect on a Group of Square Cylinders with Variable Transverse and Longitudinal Spacing", The Institution of Engineers, Bangladesh, Vol. 9.No.1, January, 1981, pp. 33-39.

[21] Mandal, A. C. and Islam, O., "A Study of Wind Effect on a Group of Square Cylinders with Variable Longitudinal Spacing", Mechanical Engineering Research Bulletin, BUET, Dhaka, Vol. 3, No. 1, 1980, pp. 21-26.

[22] Matsumoto, M., “The Dynamical Forces Acting on the Vibrating Square Prism in a Steady Flow”, Proceedings of the 3rd international Conference on Wind Effects on Buildings and Structures, Tokyo, Japan, pp. 921-930.

[23] Nakamura, Y. and Matsukawa, T., “Vortex Excitation of Rectangular Cylinders with a long side normal to the Flow”, Journal of the Fluid Mechanics, Vol. 137, 1987, pp. 171-191.

[24] Nakamura, Y. and Ohya, Y., “The Effects of Turbulence on the Main Flow past Square Rods”, Journal of Fluid Mechanics, Vol. 137, 1983, pp. 331-345.

[25] Nakamura, Y. and Yujioha, “Vortex Shedding from Square Prisms in Smooth and Turbulent Flows”, Journal of Fluid Mechanics, Vol. 164, 1986, pp. 77-89.

[26] Roberson, J. A, Chi Yu Lin, Rutherford, G. S. and Stine, M. D., “Turbulence Effects on Drag of Sharp- edged Bodies”, Journal of Hydraulics Division, Vol. 98, No. HY7, pp. 1187-1201.

[27] Roberson, J. A, Crowe, C. T and Tseng, R., “Pressure Distribution on Two and Three Dimensional Models at Small Angles of Attack in Turbulent flow”, Proceeding of the 2nd U.S. National Conference on Wind Engineering Research, June 22-25, 1975, Colorado.

[28] Shakamoto, H. and Arie, M., “Vortex Shedding from a Rectangular Prism and a Circular Cylinder Placed Vertically in turbulent Boundary Layer”, Journal of Fluid Mechanics, Vol. 126, 1983, pp. 147-165.

[29] Vickery, B. J., “Fluctuating Lift and Drag on a Long Cylinder of Square Cross section in a Smooth and in a Turbulent Stream”, Journal of Fluid Mechanics, Vol. 25, 1966, pp. 481-491.

[30] Whitbread, R. E. “Model Simulation of Wind Effects on Structures”, Proceedings of a Symposium on Wind Effects on Buildings and Structures, Teddington, U.K., 1963, pp. 283-301.

[31] Hayashi, M. Akirasakurai and Yujiohya., “Wake interference of a Row of Normal Flat Plates Arranged Side by Side in a Uniform Flow”, Journal of Fluid Mechanics, Vol. 164, 1986, pp. 1-25.

[32] Okajima, A., “Strouhal Numbers of Rectangular Cylinders”, Journal of Fluid Mechanics, Vol. 123, 1982, pp. 379-398.

[33] Cochran, L. S., and Cermak, J. E., "Full and Model Scale Cladding Pressures on the Texas Tech University Experimental Building", J. Wind Eng Ind Aerodyn. No. 43, 1992, pp. 1589-1600.

[34] Islam, T., "An Experimental Investigation of Wind Effect on Rectangular Cylinders", M.Sc. Engg. Thesis, Department of Mechanical Engg. , BUET, 1988.

[35] Sultana, K. R., "An Experimental Investigation of Wind Load on Tall Buildings with Hexagonal Cross-Section", M.Sc. Engg. Thesis, Department of Mechanical Engg., BUET, 2009.

[36] Hossain, M. J., Islam, M. Q., and Ali, M., "An Experimental Investigation of Wind Load on Tall Buildings with Octagonal Cross-Section", International Journal of Renewable Energy Research, Vol. 3, No. 1, 2013.

[37] Nakamura, Y., and Yujioha., "Vortex Shedding from Square Prisms in Smooth and Turbulent Flows," Journal of Fluid Mechanics, Vol. 164, 1986, pp. 77-89.

[38] Steggel, N., "A Numerical Investigation of the Flow Around Rectangular Cylinders," Doctor of Philosophy Thesis, School of Mechanical and Materials Engg., The University of Surrey, Guildford GU2 5XH, United Kingdom, 1998.

[39] Bearman, P. W. and Wadcock, A. J., "The Interaction between a pair of Circular Cylinders Normal to a Stream", Journal of the Fluid mechanics", Vol. 61, 1973, pp. 499-511.

[40] Lawson, T. V., "Wind Loading of Buildings, Possibilities from a Wind Tunnel Investigation", University of Bristol, U.K. Report on TVL /731A, August, 1975.

[41] Cochran, L. S. and Cermak, J. E., "Full and Model Scale Cladding Pressures on the Texas Tech University Experimental Building," J. Wind Eng Ind Aerodyne No.43, 1992, pp. 1589-1600.

[42] Franc, N., "Model Law and Experimental Technique for Determination of Wind Loads on Buildings", 1st International Conferences on Wind Effects on Building and Structure, Teddington, London 1963, HMSO.

[43] Mandal, A. C., "A study of Wind Effects on Square Cylinders", M.Sc. thesis BUET, 1979.

[44] Lamb, H, Hydrodynamics, Cambridge University Press, 1932.

[45] Lanoville, A., Gateshore, I. S. and Parkinsoon, G. V., "An Experimental of Some Effects of Turbulence on Bluff Bodies", Proceeding of the 4th International

Conference on Wind Effects on Buildings and Structure, London, U.K. 1975, pp. 333-341.

[46] Maskell, E. C., "A Theory of Blockage Effects on Bluff Bodies and Stalled Wings in a Closed Wind Tunnel", ARC R&M No. 3400, 1965, HMSO.

[47] Mchuri, F. G. et al, "Effects of the Free Stream Turbulences on Drag Coefficients of Bluff Sharp- Edged Cylinders", Nature, Vol. 224, No. 5222, November 29, 1969, pp. 908-909.

[48] Pope, A. and Haper, J. J., "Low Speed Wind Tunnel Testing", John Willy and Sons, New York, 1996.

[49] Parkinson, G. V. and Modi, V. J., "Recent Research on Wind effects on Bluff Two Dimensional Bodies", Proceedings, International Research Seminar, Wind Effects on Buildings and Structures, Ottawa, Canada, 1967, pp. 485-514.

[50] Robertson, J. M., "Pressure field at Reattachment of Separated flows", Proceeding of the 2nd U.S. National Conference on Wind Engineering Research, June 22-25, 1975, Colorado.

[51] Surry, D., "Pressure Measurements on the Texas Tech Buildings, Wind Tunnel Measurements and Comparison with Full Scale", J. Wind Eng. Ind. Aerodynamics. No. 38, 1991, pp. 235-247.

[52] Rizia, M.M, "Wind Effect on Cylinders of Pentagonal, Hexagonal and Octagonal Sections at Different Positions", M.Sc. thesis, MIST, 2018.